CAPITAL UNIVERSITY OF SCIENCE AND TECHNOLOGY, ISLAMABAD

Scattering from an Elastic Plate in a 3-Dimensional Rectangular Waveguide

by

Habiba Niaz

A thesis submitted in partial fulfillment for the degree of Master of Philosophy

in the

Faculty of Computing
Department of Mathematics

2025

I dedicate this effort to my Family, my dear Parents, my elegant Teachers and my supervisor Dr.Abdul Rehman Kashif who are always source of inspiration for me and their contributions are uncounted.

CERTIFICATE OF APPROVAL

Scattering from an Elastic Plate in a 3-Dimensional Rectangular Waveguide

by

Habiba Niaz

(MMT231002)

THESIS EXAMINING COMMITTEE

S. No.	Examiner	Name	Organization
(a)	External Examiner	Dr. Muhammad Ayub	QAU, Islamabad
(b)	Internal Examiner	Dr. Samina Rashid	CUST, Islamabad
(c)	Supervisor	Dr. Abdul Rehman Kashif	CUST, Islamabad

Dr. Abdul Rehman Kashif
Thesis Supervisor
August, 2025

Dr. Muhammad Sagheer
Head
Dept. of Mathematics
August, 2025

Dr. Muhammad Abdul Qadir
Dean
Faculty of Computing
August, 2025

Author's Declaration

I, **Habiba Niaz** hereby state that my MPhil thesis titled "**Scattering from an Elastic Plate in a 3-Dimensional Rectangular Waveguide**" is my own work and has not been submitted previously by me for taking any degree from Capital University of Science and Technology, Islamabad or anywhere else in the country/abroad.

At any time if my statement is found to be incorrect even after my graduation, the University has the right to withdraw my MPhil Degree.

(Habiba Niaz)

Registration No: MMT231002

Plagiarism Undertaking

I solemnly declare that research work presented in this thesis titled "**Scattering from an Elastic Plate in a 3-Dimensional Rectangular Waveguide**" is solely my research work with no significant contribution from any other person. Small contribution/help wherever taken has been duly acknowledged and that complete thesis has been written by me.

I understand the zero tolerance policy of the HEC and Capital University of Science and Technology towards plagiarism. Therefore, I as an author of the above titled thesis declare that no portion of my thesis has been plagiarized and any material used as reference is properly referred/cited.

I undertake that if I am found guilty of any formal plagiarism in the above titled thesis even after award of MPhil Degree, the University reserves the right to withdraw/revoke my MPhil degree and that HEC and the University have the right to publish my name on the HEC/University website on which names of students are placed who submitted plagiarized work.

(Habiba Niaz)
Registration No: MMT231002

Acknowledgement

I got no words to articulate my cordial sense of gratitude to Almighty Allah who is the most merciful and most beneficent to his creation. I also express my gratitude to the last prophet of Almighty Allah, Prophet Muhammad (PBUH) the supreme reformer of the world and knowledge for a human being.

I would like to be thankful to all those who provided support and encouraged me during this work.

I would like to be grateful to my thesis supervisor Dr. Abdul Rehman Kashif, for guiding. It would have remained incomplete without his endeavours. Due to his efforts, I was able to write and complete this assertation.

I would like to express my sincere appreciation to Dr. Muhammad Afzal for his continuous guidance, valuable feedback, and encouragement during the preparation of this thesis.

I would like to thank all my teachers who have guided me with knowledge and wisdom throughout my studies. Their support and encouragement have helped me grow academically and professionally.

I would like to pay great tribute to my parents, for their prayers, moral support, encouragement and appreciation. Last but not the least, I want to express my gratitude to my friends who helped me throughout my MPhil degree

(Habiba Niaz)

Registration No: MMT231002

Abstract

This study explores wave propagation in a duct with an elastic plate at the interface. The mathematical framework is based on the Helmholtz equation, which describes the acoustic potential in different regions while satisfying the necessary boundary conditions. Using eigenfunction expansions, the solutions are decomposed into distinct modes in each region. The interaction between the acoustic field and the elastic plate is analyzed through the Galerkin method, enabling the determination of unknown mode amplitudes. The plate dynamics are governed by the biharmonic equation, incorporating both structural and fluid interaction effects. By applying boundary and continuity conditions at the interface, a system of coupled equations is formulated, leading to expressions for transmission and reflection coefficients. This study provides valuable insights into acoustic-structure interactions, offering a foundation for analyzing sound transmission in ducts with elastic boundaries. The proposed solutions and numerical framework have applications in noise control, aeroacoustics, and structural health monitoring.

Contents

List of Figures

Abbreviations

BVPs	Boundary value problems
FMPPs	Flexible micro-perforated panels
LRs	Local resonators
MM	Mode-Matching technique
MMPPs	Metamaterial-based micro-perforated panels
OR	Orthogonality relation

Symbols

a	Length
b	Width
c_0	Sound speed
D_p	Cavity of depth
h	Thickness
E_p	Young's modulus
η_{mn}	Mode wave number
ω	Angular frequency
ϕ	Resulting perforation ratio
Z	Impedance
Z_{mn}	Modal impedance
ω_{mn}	Resonance frequency
$\mathrm{l}\boldsymbol{\psi_{mn}}$	Eigenfunction
A_{mn}	Amplitude of propagating mods
δ_{mn}	Kronecker delta
α	Fluid loading parameter
μ	Elastic plate wave number
t	Harmonic time dependence
$\bar{v}$	Average normal velocity
$\Delta\bar{p}$	Net pressure difference
v	Local normal velocity

Chapter 1

Introduction

The study of acoustics and wave behavior explores various materials and techniques used to control sound in different environments. KinslerIt et al.
[1] begin by introducing the concept of panels, which are flat or curved components embedded into surfaces such as doors, walls, or ceilings. The focus then shifts to micro-perforated panels (MPPs),which are designed to absorb sound energy and reduce reverberation in spaces like auditoriums and recording studios.

Maa [2] examines the working principle of (MPPs), along with their sound absorption capabilities and advantages. In addition, impedance conditions are discussed, explaining how sound waves interact with different surfaces, ranging from soft and rigid conditions to spring-like, free, and simply supported conditions.
Key acoustic properties, such as amplitude, frequency, and tension in sound waves, are also explored, highlighting their role in sound propagation and control.
The phenomenon of resonance is addressed, with examples such as mechanical, electrical, and acoustic resonance.

Beranek and Mellow [3] lastly introduce the Mode-Matching (MM) method, which is a crucial technique for analyzing wave reflection, transmission, and absorption in waveguides. The method involves analyzing the behavior of a system with simply supported boundary conditions, specifically for (MMPPs) under harmonic excitation.It begins with deriving the displacement functions for both spatial dimensions (x and y) of the system and proceeds to determine their eigenfunctions.

The analysis then applies the boundary conditions to find the eigenvalues and eigenfunctions, leading to the formulation of displacement equations for the system.

Leissa [4] investigates the calculation of partial derivatives of displacement with respect to time and spatial coordinates, which are essential for understanding the dynamic response of the system. Structural damping is incorporated into the model, and the study derives the relationships between the system's displacement, velocity, and impedance.

This leads to the formulation of an impedance matrix that accounts for factors such as resonance frequencies and damping effects.

Considering the orthogonality relations between the eigenfunctions, the system's impedance is computed by integrating over the panel's surface area. The study concludes with the computation of the average velocity of the system and the impedance of the micro-perforated panel, providing valuable insights into the panel's dynamic behavior. This analysis is crucial for designing efficient acoustic materials and understanding how structural properties affect sound absorption and control.

The dynamic behavior of a system subjected to external forces is analyzed by applying appropriate boundary conditions and governing differential equations. The focus is placed on the elastic plate dynamics and the interaction between different regions in the system, particularly regions I and II. This involves studying wave propagation, modal analysis, and displacement functions under various boundary conditions.

Rao [5] applies the superposition principle to solve for the potential field in both regions, formulating eigenvalue problems to account for spatial and temporal evolution.

These problems are solved through the introduction of arbitrary constants, allowing the representation of different vibration modes.

Trigonometric functions are used to represent these modes, and boundary conditions are applied to determine the eigenvalues. The displacement functions for both regions are derived, and the total field potential

is expressed as a sum over all possible modes. The interaction between the fluid in region I and the plate in region II is modeled using the Galerkin method, which facilitates the calculation of the unknown coefficients describing the amplitude of each mode. Further analysis explores the dynamic response of the elastic plate, incorporating the Galerkin formulation to solve for the unknown amplitudes. This analysis extends to consider factors such as resonance frequencies, damping, and the interaction at the interface between the fluid and the plate, ultimately providing a comprehensive understanding of the system's behavior. This approach offers valuable insights for engineering applications involving (MMPPs) and elastic plates, contributing to an understanding of how structural properties influence wave propagation, resonance, and damping. These findings are relevant to applications such as acoustic treatment, noise control, and the design of materials in structural dynamics.

1.1 Literature Review

Ren et al. [6] introduced a novel kind of perforated sound absorber known as (MMPPs), along with the sound-absorbing capabilities of flexible micro-perforated panels (FMPPs). Local resonators (LRs), attached at a sub-wavelength scale, are combined with a micro-perforated host panel in (MMPPs) to target flexural waves. Simulations, both theoretical and numerical, demonstrate that (MMPPs) can significantly increase sound absorption throughout a broad frequency range.

Yeang et al. [7] reported that arranging multiple resonators in a circular configuration enhances uniform coupling between the resonators and the (MPP). This arrangement leads to a more consistent sound absorption coefficient over a targeted frequency range. Their experimental findings demonstrated that, by using a supported panel with circularly distributed multi-frequency resonators, the (MPP) achieved a wide low-frequency half-bandwidth of approximately 160–550 Hz.

Yeang et al. [8] compared to a single (MPP) structure, the experimental findings showed a significant improvement in the mean absorption coefficient at extremely low frequencies. Zhang et al. [9] demonstrated that the absorption performance of

the micro-perforated panel can be enhanced by adding additional local resonators, and that the absorption bandwidth can be effectively widened by varying the mass ratio or the spring stiffness.

Mu et al. [10] provided a more accurate prediction of sound absorption for the practical application of (MMPP) in complex environments.

Gai et al. [11] showed that micro-perforated panels can reduce the loss of sound insulation caused by mass-air-mass resonance in multi-layer structures. To improve sound absorption in single-layer (MPPs), they proposed a new design called (MPPHR), which combines (MPPs) with Helmholtz resonators. Simulations and experiments showed that (MPPHR) has two peak frequencies and one anti-resonant frequency. Sakagami et al. [12] conducted a parametric numerical analysis to examine the influence of different control parameters. They also discussed potential design strategies and the underlying absorption mechanisms. The results indicated that substantial additional absorption could be obtained in the low-frequency range, while a resonant absorption behavior—comparable to that of traditional (MPP) absorbers—was observed at mid to high frequencies. This low-frequency absorption characteristic, resembling that of a double-leaf permeable membrane, offers performance benefits over standard (MPP) configurations.

Mosa et al. [13] found that placing two (MPPs) one after the other creates a double-layer design, which can absorb sound over a wider range of frequencies. They also suggested that using holes of different sizes could make this range even bigger.

Prasetiyo et al. [14] introduced a coiling structure in the backing air cavity to achieve a thinner micro-perforated panel (MPP) for the same desired operating frequency. Additionally, a parallel setup with several sub-(MPPs) was used to trigger multiple resonances, thereby expanding the overall absorption bandwidth. Small holes were added to mitigate the large dips typically found in such arrangements. The evolution of broadband and thin (MPPs) is described, supported by both experimental and theoretical findings.

Toyoda and Furthermore [15] highlighted additional advantages of (MPPs) , such as being hygienic, aesthetically pleasing, and environmentally friendly. (MPPs) are therefore very promising substitutes for the next generation of sound absorbers.

To predict (MPP) performance, analytical and numerical approaches such as computational fluid dynamics, boundary element method, and finite element method have been employed Ma et al. [16] developed a two-port system with quasi-perfect absorption is built using (MPP) resonators. In contrast to one-port systems, where reducing reflected waves might achieve near-unity absorption, the symmetry of a two-port system limits the absorption coefficient of a single resonator to 0.5. However, near-unity absorption over a wide frequency range can be obtained by linking several resonators to concurrently achieve near-zero transmission and reflection.

Liu et al. [17] used a network analyzer to experimentally assess the transfer function of the proposed absorber's shunt circuit. The sound absorption coefficients were also determined using an impedance tube and the two-microphone transfer function method.

Zhang et al. [18] presented experimental techniques and theoretical foundations for the design and application of curved micro-perforated panel metamaterials. Hashemi et al. [19] evaluated the average normal sound absorption coefficient (SAC) in the 125–3000 Hz frequency range. QianIn et al. [20] noted that in noise control engineering, (MPP) absorbers are growing in popularity, as they are positioned to be the basis for the next generation of sound-absorbing materials. To facilitate the design of (MPP) absorbers' structural parameters in accordance with specific requirements, a straightforward method for predicting their absorption performance is required.

Gai et al. [21] anticipated that the next generation of sound-absorbing materials would be constructed using (MPP) absorbers, which are gaining popularity in the field of noise control engineering. The development of (MPP) absorbers' structural parameters according to specific requirements requires a straightforward method for predicting their absorption performance. Toyoda et al. [22] investigated a circular duct containing a finite flexible (MPP). The predicted results were experimentally validated using an acoustic tube to measure the absorption coefficient under normal incidence. The analysis shows that Helmholtz-resonance absorption is not influenced by panel-type absorption, which is caused by the panel's eigenmode vibrations. However, with respect to the perforation ratio, panel-type absorption—induced by the mass-spring resonance of the panel and the

rear cavity—exhibits a trade-off with Helmholtz-resonance absorption. Sakagami et al. [23] found that the honeycomb structure does not affect the additional low-frequency absorption characteristics of double-layer micro-perforated panels (DLMPPs), but it does enhance the sound absorption performance of (DLMPPs) near the resonance peak. Xu et al. [24] introduced an extended theoretical model for (MPPs), generalizing Maa's original theory for circular perforations to include petal-shaped configurations. Guo and Min [25] discussed the acoustic performance of the proposed structure, which achieved a peak absorption

coefficient of 0.9, demonstrating its high efficiency in the target frequency range. Arndt [26] provided a comprehensive review of recent developments in mode-matching (MM) techniques, highlighting their application in fast and accurate computer-aided design (CAD) and waveguide component optimization.

Kirilenko et al. [27] proposed a method to compute waveguide (WG) circuits with smooth boundaries, which can be approximated by a staircase surface, as well as those with metallic boundaries defined in the Cartesian coordinate system. The proposed method enables calculations for both cases. The corresponding electromagnetic solvers offer a compromise between the high precision and computational efficiency of specialized mode-matching techniques and the universality of mesh-based approaches.

Dreher [28] proposed a systematic mode-matching approach that reduces the complexity of acoustic analysis by lowering both analytical derivations and numerical computations.

This method provides an efficient balance between accuracy and computational cost, which makes it highly suitable for dealing with practical engineering problems. By organizing the procedure in a structured way, the approach simplifies the modeling of wave interactions in ducts and waveguides, thereby extending the applicability of mode-matching techniques to real-world acoustic systems. Polo [29] extended mode-matching techniques to effectively address challenges related to lateral and transverse wall boundary conditions in waveguide constructions. Vale and Meyer [30] proposed a novel mode

selection strategy to enhance computational efficiency in mode-matching problems, significantly reducing system size without compromising accuracy. Franza and Chew [31] developed a recursive algorithm designed to adaptively select the optimal number of modes in each waveguide segment, after analyzing various waveguide geometries using the mode-matching approach.
Numerical simulations for a range of applications are provided, demonstrating excellent agreement and validating the methodology. Llorente et al. [32] developed a generalized mode-matching method to deal with acoustic wave propagation in structures that cannot be easily analyzed using a single coordinate system. In particular, they considered geometries made up of axially uniform guides together with radial waveguides,which normally require different mathematical treatments. By combining these two coordinate systems in a unified way, their approach makes it possible to study more complex and realistic configurations than traditional methods allow. This technique is especially useful for analyzing hybrid acoustic structures, where the interaction between different parts of the geometry plays an important role in the overall wave behavior. This work provides a strong foundation for extending mode-matching techniques to a wider range of engineering applications.

1.2 Thesis Contribution

The primary contributions of this thesis to the field of acoustic–structure interaction and waveguides include the development of a comprehensive analytical and numerical framework for evaluating the acoustic impedance of an elastic plate embedded in a rigid, infinite rectangular waveguide using a combination of the Mode–Matching and Galerkin methods. This formulation accounts for structural damping and modal coupling effects. The study was further extended to a three-dimensional rectangular waveguide with an elastic plate at the interface of two fluid-filled regions, considering both rigid-wall and soft-wall backing conditions.

This dual-case analysis allows a direct comparison of the influence of boundary compliance on vibroacoustic coupling.

Closed-form expressions for eigenfunctions, eigenvalues, and modal impedances were derived for the simply supported panel configuration and incorporated into a solvable system of algebraic equations for numerical evaluation. The derived formulations were implemented in Mathematica to obtain numerical results for specific geometric and material parameters, retaining a finite number of modes (N = 16) for accurate yet computationally efficient simulations.

A detailed numerical comparison between rigid and soft wall configurations was provided, showing that soft boundaries yield broader and deeper absorption dips, whereas rigid boundaries produce narrow-band resonances with higher reflection.

Visualizations of the modal pressure and velocity fields in three dimensions were also presented for both configurations, offering physical insight into the interaction between the elastic plate and the surrounding acoustic field.

Overall, this research offers both theoretical and practical tools that can assist in the design of advanced acoustic materials and noise-control systems.

1.3 Thesis Layout

This thesis contains five chapters.

- **Chapter 1** introduces the study and presents a detailed review of previous research. It explains the key concepts and findings from earlier work that form the basis for this research.
- **Chapter 2** introduces preliminary concepts and definitions that are useful for understanding the material presented in the remaining chapters.
- **Chapter 3** presents the simply supported panel frame with an (MPP). It develops equations for x and y displacement, determines eigenfunctions, and forms displacement functions.

It also examines structural damping, calculates impedance, and analyzes modal behavior, resonance frequencies, and average velocity.

- **Chapter 4** investigates wave propagation in a fluid-filled duct and the response of an elastic plate at the interface of two regions. The wave equations in both regions are solved using the separation of variables method, while the Galerkin method is used to find unknown coefficients. Eigenfunctions, wave numbers, and boundary conditions are applied to model the system, and the plate's deflection is determined through an eigenvalue problem. The chapter offers a detailed study of the wave behavior and plate dynamics.

- **Chapter 5** Provides the concluding remarks of the study, followed by a bibliography listing all references cited in the thesis.

Chapter 2

Perliminaries

This chapter provides the groundwork with fundamental definitions and laws, providing a valuable resource for subsequent chapters.

2.1 Acoustic

"Acoustics is a branch of physics that studies mechanical waves—like sound, vibrations, ultrasound, and infrasound—as they travel through gases, liquids, and solids" [33].

Acoustic mode-matching methods are widely used to study how sound waves behave in ducts, waveguides, and other confined geometries. These approaches help in accurately predicting wave reflection, transmission, and coupling effects in complex acoustic structures.

2.2 Acoustic Wave Equation

To understand how sound waves move through the air, we use math equations based on basic principles like mass, momentum, and energy. However, these equations can be complex and hard to analyze. To make it simpler, we use a linear

approximation, which helps us understand how sound waves behave in the air.The wave equation is a fundamental mathematical model in acoustics, used to describe the propagation of sound through a medium :

$$\frac{\partial^2 p}{\partial t^2} = c^2 \nabla^2 p. \tag{2.1}$$

2.2.1 Conservation of Mass

"The conservation of mass equation is a fundamental principle in physics that describes how the mass of a substance changes over time within a specific area. This equation helps us understand how the mass density of a substance changes due to the flow of mass into or out of that area". [34]:

Mathematically, this can be stated as:

$$\frac{\partial \rho}{\partial t} + \nabla \cdot (\rho \mathbf{u}) = 0, \tag{2.2}$$

where ρ is the density, ∇ stands for the divergence operator and $\mathbf{u}$ represents the velocity field.

2.2.2 Conservation of Momentum

"The conservation of momentum equation is a fundamental principle in physics that describes how the momentum of a system changes when forces are applied. It connects the system's forces and the net momentum flow rate" [35].

Mathematically, this can be stated as:

$$\frac{\partial (\rho \mathbf{u})}{\partial t} = -\nabla \cdot (\rho \mathbf{u}\mathbf{u}) - \nabla p + \rho \mathbf{g}, \tag{2.3}$$

where ρ denotes the density, $\mathbf{u}$ stands for the velocity,

p denotes the pressure, and $\mathbf{g}$ represents the gravitational acceleration. Applying the continuity condition, we can express the conservation of momentum equation as:

$$\rho \frac{D\mathbf{u}}{Dt} = -\nabla p + \rho \mathbf{g}, \tag{2.4}$$

where ($\frac{D}{Dt} = \frac{\partial}{\partial t} + \mathbf{u} \cdot \nabla$) represents the total time derivative, also known as the Stokes total derivative.

2.3 Micro-Perforated Panels

2.3.1 Definition

"Micro-Perforated Panels (MPPs) are sound absorbing materials that use a panel with very small perforations (typically less than 1 mm in diameter) to dissipate acoustic energy through viscous losses in the perforations, without the use of fibrous materials.
MPPs are widely used in noise control applications due to their durability, cleanability, and effectiveness over a broad frequency range" [36]. Micro-perforated panels (MPPs) are widely used in acoustics because they provide effective sound absorption without the need for traditional porous materials. Their performance mainly depends on factors such as hole diameter, perforation ratio, panel thickness, and the depth of the backing cavity.

Working Principle:

Micro-perforated panels work by allowing sound waves to pass through the tiny holes, where they are absorbed by a porous material, such as fiberglass or mineral wool. This process involves three stages: 1. Sound waves pass through the perforations and enter the panel.
2. The sound energy is absorbed by the porous material, converting it into

heat energy.

3. As the heat energy dissipates, less sound energy is reflected back into the space.

2.3.2 Sound Absorption Coefficient

The sound absorption coefficient, denoted by α, represents the portion of the incoming sound energy that is absorbed by a material instead of being reflected back. It quantifies how effectively a surface dissipates acoustic energy, and its value ranges between 0 (perfect reflection) and 1 (perfect absorption). It is mathematically defined as:

$$\alpha = 1 - \left| \frac{p_r}{p_i} \right|^2 ,$$

where p_r is the reflected sound pressure amplitude and p_i is the incident sound pressure amplitude.

It can also be expressed in terms of acoustic impedance Z as:

$$\alpha = 1 - \left| \frac{Z - Z_0}{Z + Z_0} \right|^2 ,$$

where Z is the surface acoustic impedance and Z_0 is the characteristic impedance of air [37]. The sound absorption coefficient is a measure of how effectively a material or surface absorbs incident sound energy.

2.4 Boundary Conditions in Acoustics and Structural Dynamics

Boundary conditions describe how a structure or medium interacts with waves at its boundaries. Below are common types:

2.4.1 Impedance Condition

The impedance boundary condition relates the acoustic pressure p to the normal particle velocity u_n through the surface impedance Z_s:

$$p = Z_s u_n,$$

where Z_s is the specific acoustic impedance of the surface [38]. These are type of boundary impedance.

2.4.2 Soft boundary Condition

A soft or pressure-release boundary assumes zero acoustic pressure:

$$p = 0,$$

This models surfaces such as open ends in ducts [38]. This type of boundary is commonly used to represent open duct ends or surfaces where the medium is directly exposed to the atmosphere. A soft boundary condition in acoustics represents a surface where the sound pressure vanishes. Such boundaries are generally used to describe open terminations or surfaces that behave like perfect absorbers.

2.4.3 Rigid boundary Condition

A rigid boundary assumes zero normal particle velocity:

$$u_n = 0,$$

This corresponds to perfectly reflecting surfaces [38].A rigid boundary condition describes a surface that does not allow particle motion, meaning the normal component of acoustic velocity is zero at the wall. This type of condition is commonly used to model perfectly reflecting surfaces in ducts and waveguides.

2.4.4 Edge boundary Condition

An edge boundary condition defines the physical constraints imposed along the edges of a structural element such as a plate or beam.
Depending on the problem, the edge may be treated as fixed, simply supported, free, or elastically restrained, each of which influences the vibration and acoustic response of the structure. [38].

2.4.5 Spring-like boundary Condition

A spring-like boundary follows Hooke's law:

$$F = k\, w,$$

where k is the spring constant and w is the displacement [38].
A spring-like boundary condition assumes that the edge of the structure is supported by an elastic restraint. The restoring force at the boundary is proportional to the displacement, with the stiffness of the spring controlling the level of flexibility at the support.

2.4.6 Fixed boundary Condition

A fixed (clamped) boundary has:

$$w = 0, \quad \frac{\partial w}{\partial n} = 0.$$

This constrains both displacement and slope [38].
The plate cannot move at the edge and its rotation (slope) is also completely restricted. A fixed boundary condition is one in which the displacement of the structure is restricted to zero along the boundary.

2.4.7 Free boundary Condition

A free boundary satisfies:

$$M = 0 \quad and \quad Q = 0,$$

where M is bending moment and Q is shear force [38] .This represents a boundary that is not restrained and can move freely without resistance.

2.5 Basic Acoustic and Vibration Terms

Waveguide

"A waveguide is a structure that directs the propagation of waves, such as sound or electromagnetic waves, along a desired path". Mathematically, wave propagation in a rigid-walled acoustic waveguide satisfies the Helmholtz equation:

$$\nabla^2 p + k^2 p = 0,$$

where p is acoustic pressure and $k = (\frac{\omega}{c})$ is the wave number [39].

2.5.1 Amplitude

"Amplitude is the maximum displacement of a wave from its equilibrium position". The amplitude indicates the peak value of the oscillation and is associated with the wave's energy higher amplitudes correspond to greater amounts of energy being transmitted.

$$y(t) = A\sin(\omega t + \phi),$$

where A is the amplitude [39]. Amplitude is the maximum value of oscillation, and larger amplitudes show that the wave carries more energy.

2.5.2 Time Period

"The time period T is the duration of one complete cycle of a wave":

$$T = \frac{1}{f},$$

where f is the frequency [39]. Time period inversely related to frequency, meaning shorter time periods correspond to higher frequencies.

2.5.3 Frequency

"Frequency is the number of oscillations per unit time":

$$f = \frac{\omega}{2\pi},$$

where ω is the angular frequency in radians per second [39]. Frequency represents the number of oscillations or cycles completed by a wave or system in one second.

2.5.4 Resonance

"Resonance occurs when a system is driven at a frequency equal to its natural frequency, resulting in maximum amplitude" [40].

2.5.5 Natural Frequency

The natural frequency f_n of a simple mass–spring system is:

$$f_n = \frac{1}{2\pi}\sqrt{\frac{k}{m}},$$

where k is stiffness and m is mass [40]. This frequency is a key property of the system, as it depends only on its physical parameters. Increasing the stiffness raises the natural frequency, while increasing the mass lowers it.

2.5.6 Resonance

"Resonance is a phenomenon where a system oscillates with large amplitude when driven by an external force whose frequency matches the system's natural frequency". For a simple harmonic oscillator:

$$A(\omega) = \frac{F_0/m}{\sqrt{(\omega_n^2 - \omega^2)^2 + (2\zeta\omega_n\omega)^2}},$$

where F_0 is force amplitude, ω_n is natural angular frequency, and ζ is damping ratio [40].

2.5.7 Mode Matching

Mode matching is a method used to analyze wave propagation problems by representing the solution in each region as a sum of modes that satisfy the local boundary conditions. The modes from adjacent regions are then connected through continuity requirements at their shared boundaries. This approach simplifies complex geometries into manageable sections, making it possible to obtain accurate solutions for scattering and transmission problems. It is especially useful in duct acoustics and waveguides, where discontinuities or changes in geometry strongly influence the behavior of the propagating waves.

2.5.8 Metamaterial-based Micro-Perforated Panels

Metamaterial-based Micro-Perforated Panels (MMPPs) are engineered structures combining micro-perforations with metamaterial effects to improve acoustic absorption and noise control [41].

Chapter 3

Acoustic Impedance of an Elastic Plate in Rigid Infinite Waveguide

3.1 Introduction

This chapter focuses on the detailed analysis of a simply supported panel frame that incorporates a micro-perforated panel with metamaterial properties (MMPP). The study investigates its harmonic displacement and overall behavior when subjected to structural forces and acoustic loading. The discussion begins with the derivation of the governing equations for displacement in both the and directions, applying the boundary conditions appropriate for a simply supported configuration. These formulations lead to the determination of eigenfunctions and dispersion relations for each direction, ultimately producing the general form of the panel's displacement functions. A harmonic representation of the displacement field is then developed, from which velocity expressions, displacement derivatives, and associated governing relations are obtained. The concept of structural damping is incorporated by introducing a damping factor into the governing equations, allowing for the evaluation of the mechanical impedance of the panel frame. The analysis also addresses the effect of panel material properties

geometric parameters and boundary constraints on thedynamic response of the (MMPP). Special attention is given to the coupling between the panel's structural modes and the acoustic field inside the surrounding waveguide, emphasizing the role of modal interaction in sound absorption and energy dissipation. Furthermore, the chapter investigates the resonance frequencies, mode shapes, and frequency-dependent impedance behavior of the (MMPP). It derives closed-form expressions for average surface velocity, which are essential for computing sound transmission loss and absorption performance. The results from this theoretical framework serve as the basis for numerical simulation and provide key insights for optimizing (MMPP) designs in practical acoustic applications.

3.2 Problem Formulation

A rectangular waveguide with a elastic plate located at the plane $\bar{z} = 0$ is considered, as shown in Figure (3.1).

Between the sound pressure excitation, the (MMPP), and the closed cavity, the vibroacoustic coupling dynamic equilibrium equation is governed by the following equation,

$$D_p \Delta^4 W(x, y, t) + \rho_{eff}(\omega) h \frac{\partial^2 W(x, y, t)}{\partial t^2} = (p - p_D) e^{i\omega t} \ . \tag{3.1}$$

In this equation, p is the uniformly distributed sound pressure on the lower face of the (MMPP), while p_D is the distributed pressure on its upper face. Additionally, operator Δ^4 in rectangular coordinate is:

$$\Delta^4 = \left(\frac{\partial^2}{\partial x^2} + \frac{\partial^2}{\partial y^2} \right)^2 = \left(\frac{\partial^4}{\partial x^4} + \frac{\partial^4}{\partial y^4} + 2 \frac{\partial^4}{\partial x^2 \partial y^2} \right).$$

The flexural rigidity of the host panel is denoted by D_p and is defined as:

$$D_p = \frac{E_p h^3}{12(1 - \nu^2)},$$

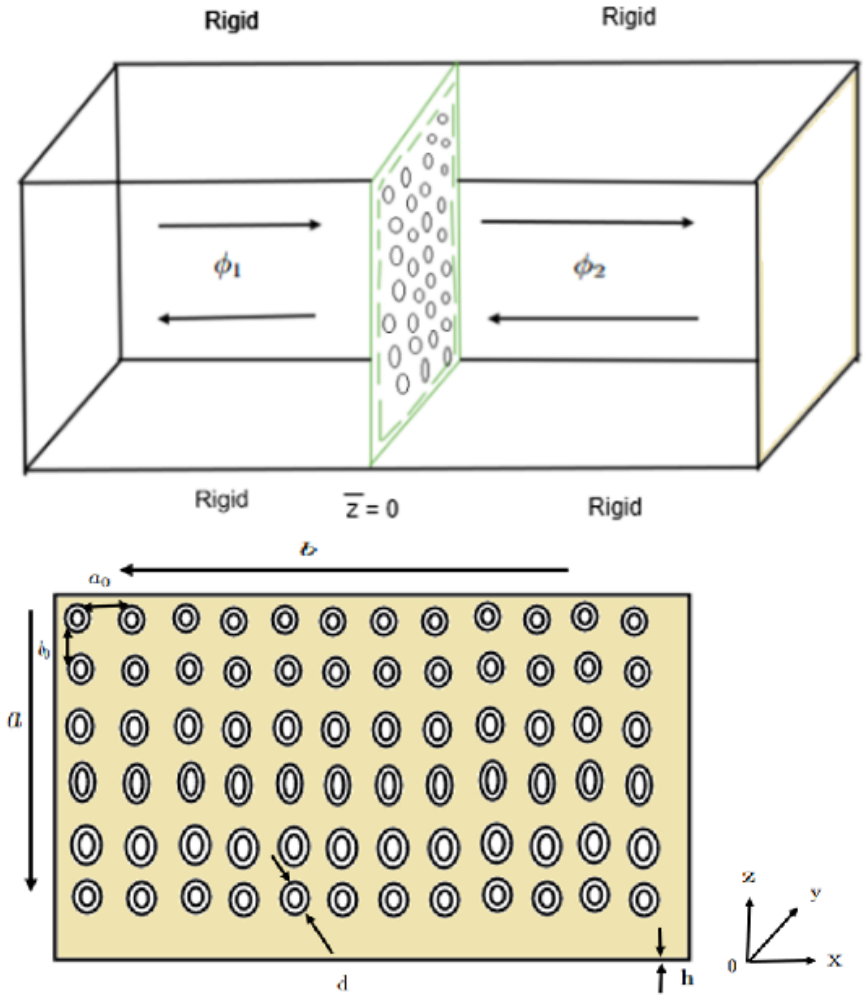

FIGURE 3.1: Physical structure of the waveguide

where E_p is the Young's modulus of the host panel, and $W(x, y, t)$ is the out-of-plane displacement of the host panel, and the quantity $\rho_{eff}(\omega)$ is the effective dynamic mass density of (MMPP).

For a simply supported rectangular plate, the boundary conditions are:

$$W(0, y, t) = 0, \tag{3.2}$$

$$W(a, y, t) = 0, \tag{3.3}$$

$$\frac{\partial^2 W}{dx^2}(0, y, t) = 0, \tag{3.4}$$

$$\frac{\partial^2 W}{dx^2}(a, y, t) = 0, \tag{3.5}$$

$$W(x, 0, t) = 0, \tag{3.6}$$

$$W(x,b,t)=0, \tag{3.7}$$

$$\frac{\partial^2 W}{dy^2}(x,0,t)=0, \tag{3.8}$$

$$\frac{\partial^2 W}{dy^2}(x,b,t)=0. \tag{3.9}$$

To solve equation (3.1) subject to edge conditions from equation (3.2) to equation (3.9), we write the eigenvalue problem associated with the governing differential system, that is

$$\left(\frac{\partial^4}{\partial x^4}+2\frac{\partial^4}{\partial x^2\partial y^2}+\frac{\partial^4}{\partial y^4}\right)\phi_{mn}-\lambda_{mn}^4\phi_{mn}=0, \tag{3.10}$$

$$\phi_{mn}(0,y)=0, \tag{3.11}$$

$$\phi_{mn}(a,y)=0, \tag{3.12}$$

$$\phi_{mn}''(0,y)=0, \tag{3.13}$$

$$\phi_{mn}''(a,y)=0, \tag{3.14}$$

$$\phi_{mn}(x,0)=0, \tag{3.15}$$

$$\phi_{mn}(x,b)=0, \tag{3.16}$$

$$\phi_{mn}''(x,0)=0, \tag{3.17}$$

$$\phi_{mn}''(x,b)=0. \tag{3.18}$$

Now we solve the eigenvalue problem defined in equation (3.10) to equation (3.18), we rewrite equation (3.10) as

$$\Delta^4\phi_{mn}-\lambda_{mn}^4\phi_{mn}=0, \tag{3.19}$$

or

$$(\Delta^2\phi_{mn}+\lambda_{mn}^2\phi_{mn})(\Delta^2\phi_{mn}-\lambda_{mn}^2\phi_{mn})=0. \tag{3.20}$$

To solve equation equation (3.19), we split the equation into two separate parts.We define ϕ_{1mn} as the function that satisfies:

$$\Delta^2\phi_{1mn} + \lambda_{mn}^2\phi_{1mn} = 0, \tag{3.21}$$

while ϕ_{2mn} is assumed to satisfy:

$$\Delta^2\phi_{2mn} - \lambda_{mn}^2\phi_{2mn} = 0. \tag{3.22}$$

To determine , equation (4.21) can be rearranged into a suitable form. This reformulated equation is then used to solve for the required modal coefficient.

$$\frac{\partial^2\phi_{1mn}}{\partial x^2} + \frac{\partial^2\phi_{1mn}}{\partial y^2} + \lambda_{mn}^2\phi_{1mn}(x,y) = 0. \tag{3.23}$$

Using the separation of variables method, thus we may assume

$$\phi_{1mn}(x,y) = X_{1m}(x)Y_{1n}(y). \tag{3.24}$$

Substituting equation (3.24) into equation (3.23), we get

$$\frac{\partial^2 X_{1m}}{\partial x^2}Y_{1n} + \frac{\partial^2 Y_{1n}}{\partial y^2}X_{1m} + \lambda_{mn}^2 X_{1m}Y_{1n} = 0. \tag{3.25}$$

Dividing equation (3.25) with $X_{1m}(x)Y_{1n}(y)$ leads to

$$\frac{1}{X_{1m}}\frac{\partial^2 X_{1m}}{\partial x^2} + \frac{1}{Y_{1n}}\frac{\partial^2 Y_{1n}}{\partial y^2} + \lambda_{mn}^2 = 0, \tag{3.26}$$

or

$$\frac{1}{X_{1m}}\frac{\partial^2 X_{1m}}{\partial x^2} = -\frac{1}{Y_{1n}}\frac{\partial^2 Y_{1n}}{\partial y^2} - \lambda_{mn}^2 = -\alpha^2, \tag{3.27}$$

here α is any arbitrary constant that will be found using edge conditions, equation (3.11) to equation (3.18). Now for $X_{1m}(x)$, we may write from equation (3.27) as

$$\frac{1}{X_{1m}}\frac{\partial^2 X_{1m}}{\partial x^2} + \alpha^2 = 0, \tag{3.28}$$

which can be solved to get

$$X_{1m}(x) = c_1 \cos(\alpha x) + c_2 \sin(\alpha x), \tag{3.29}$$

where c_1 and c_2 are arbitrary constants.

Under simply supported boundary conditions, we derive the corresponding relations.

$$X_{1m}(0) = 0, \tag{3.30}$$

$$X_{1m}(a) = 0, \tag{3.31}$$

$$X''_{1m}(0) = 0, \tag{3.32}$$

$$X''_{1m}(a) = 0. \tag{3.33}$$

From equation (3.29) and equation (3.30), we can write:

$$X_{1m}(0) = c_1 \cos(0) + c_2 \sin(0) = 0, \tag{3.34}$$

which yield

$$c_1 = 0. \tag{3.35}$$

Substituting $c_1 = 0$ into equation (3.29), we get

$$X_{1m}(x) = c_2 \sin(\alpha x). \tag{3.36}$$

Taking double derivative of equation (3.36),

$$X''_{1m}(x) = -\alpha^2 c_2 \sin(\alpha x). \tag{3.37}$$

From equation (3.37) and equation (3.33),

$$X''_{1m}(a) = -\alpha^2 c_2 \sin(\alpha a) = 0, \tag{3.38}$$

which yields $c_2 \neq 0$ for non trivial solution, therefore

$$c_2 \sin(\alpha a) = 0, \tag{3.39}$$

or

$$\sin(\alpha a) = 0. \tag{3.40}$$

From equation (3.40), the mathematical form of the dispersion relation is obtained, which links the system's parameters to its wave propagation characteristics. Solving this relation gives the eigenvalue, representing the specific mode's propagation constant or frequency.

$$\alpha_m = \frac{m\pi}{a}, \quad m = 1, 2, 3, \ldots \tag{3.41}$$

Substituting equation (3.41) into equation (3.36), the eigenfunctions

$$X_{1m}(x) = \sin\left(\frac{m\pi}{a}x\right), \quad m = 1, 2, 3, \ldots \tag{3.42}$$

Accordingly from equation (3.27), we can get for $Y_{1n}(y)$ as:

$$\frac{1}{Y_{1n}}\frac{\partial^2 Y_{1n}}{\partial y^2} + \lambda_{mn}^2 - \alpha^2 = 0, \tag{3.43}$$

or

$$\frac{1}{Y_{1n}}\frac{\partial^2 Y_{1n}}{\partial y^2} + \beta^2 = 0, \tag{3.44}$$

where

$$\beta^2 = \lambda_{mn}^2 - \alpha^2. \tag{3.45}$$

Now equation (3.44) can be solved to get

$$Y_{1n}(y) = c_3 \cos(\beta y) + c_4 \sin(\beta y), \tag{3.46}$$

where c_3 and c_4 are arbitrary constants. Under simply supported boundary conditions, we derive the corresponding relations.

$$Y_{1n}(0) = 0, \tag{3.47}$$

$$Y_{1n}(b) = 0, \tag{3.48}$$

$$Y_{1n}^{''}(0) = 0, \tag{3.49}$$

$$Y_{1n}^{''}(b) = 0. \tag{3.50}$$

From equation (3.46) and equation (3.47), we can write

$$Y_{1n}(0) = c_3 \cos(0) + c_4 \sin(0) = 0, \tag{3.51}$$

which yield

$$c_3 = 0. \tag{3.52}$$

Substituting $c_3 = 0$ into equation (3.46), we get

$$Y_{1n}(y) = c_4 \sin(\beta y). \tag{3.53}$$

Taking double derivative of equation (3.53), gives

$$Y_{1n}^{''}(y) = -\beta^2 c_4 \sin(\beta y). \tag{3.54}$$

From equation (3.50) and equation (3.54), we find

$$Y_{1n}^{''}(b) = -\beta^2 c_4 \sin(\beta b) = 0, \tag{3.55}$$

This condition leads to for a non-trivial solution. Therefore, the resulting equation must be satisfied to ensure a meaningful physical response.

$$\sin(\beta b) = 0. \tag{3.56}$$

From equation (3.56), we get the dispersion relation whose eigenvalue is:

$$\beta_n = \frac{n\pi}{b}, \quad n = 1, 2, 3, \ldots \tag{3.57}$$

Substituting equation (3.57) into equation (3.53), the eigenfunctions

$$Y_{1n}(y) = \sin\left(\frac{n\pi}{b}y\right). \tag{3.58}$$

Substituting equation (3.58) and equation (3.42) into equation (3.24),we get

$$\phi_{1mn}(x,y) = sin\left(\frac{n\pi}{b}y\right)\sin\left(\frac{m\pi}{a}x\right). \tag{3.59}$$

To find ϕ_{2mn}, equation(3.22) is expressed in the required form. This expression is then used to evaluate the corresponding modal coefficient.

$$\frac{\partial^2\phi_{2mn}}{\partial x^2} + \frac{\partial^2\phi_{2mn}}{\partial y^2} - \lambda_{mn}^2\phi_{2mn}(x,y) = 0. \tag{3.60}$$

Using the method of separation of variables, we may assume

$$\phi_{2mn}(x,y) = X_{2m}(x)Y_{2n}(y). \tag{3.61}$$

Substituting equation (3.61) into equation (3.60), we get

$$\frac{\partial^2 X_{2m}}{\partial x^2}Y_{2n} + \frac{\partial^2 Y_{2n}}{\partial y^2}X_{2m} - \lambda_{mn}^2 X_{2m}Y_{2n} = 0. \tag{3.62}$$

Dividing equation (3.62) with $X_{2m}(x)Y_{2n}(y)$ leads to

$$\frac{1}{X_{2m}}\frac{\partial^2 X_{2m}}{\partial x^2} + \frac{1}{Y_{2n}}\frac{\partial^2 Y_{2n}}{\partial y^2} - \lambda_{mn}^2 = 0, \tag{3.63}$$

or

$$\frac{1}{X_{2m}}\frac{\partial^2 X_{2m}}{\partial x^2} = -\frac{1}{Y_{2n}}\frac{\partial^2 Y_{2n}}{\partial y^2} + \lambda_{mn}^2 = \alpha^2. \tag{3.64}$$

Here α is any arbitrary constant that will be found using edge conditions, equation (3.11) to equation (3.18).

Now for $X_{2m}(x)$, we may write from equation (3.64) as

$$\frac{1}{X_{2m}}\frac{\partial^2 X_{2m}}{\partial x^2} - \alpha^2 = 0, \tag{3.65}$$

which can be solved to get

$$X_{2m}(x) = c_5 \cosh(\alpha x) + c_6 \sinh(\alpha x), \tag{3.66}$$

where c_5 and c_6 are arbitrary constants.

For the simply supported boundary conditions,

$$X_{2m}(0) = 0, \tag{3.67}$$

$$X_{2m}(a) = 0, \tag{3.68}$$

$$X''_{2m}(0) = 0, \tag{3.69}$$

$$X''_{2m}(a) = 0. \tag{3.70}$$

From equation (3.66) and equation (3.67), we can write

$$X_{2m}(0) = c_5 \cosh(0) + c_6 \sinh(0) = 0, \tag{3.71}$$

which yields

$$c_5 = 0. \tag{3.72}$$

Substituting $c_5 = 0$ into equation (3.66), we get

$$X_{2m}(x) = c_6 \sinh(\alpha x). \tag{3.73}$$

Taking double derivative of equation (3.73)

$$X''_{2m}(x) = -\alpha^2 c_6 \sinh(\alpha x). \tag{3.74}$$

From equation (3.74) and equation (3.70), we find

$$X''_{2m}(a) = -\alpha^2 c_6 \sinh(\alpha a) = 0, \tag{3.75}$$

This condition implies that $c_6 \neq 0$ for a non-trivial solution. Therefore, the corresponding equation must be satisfied to ensure a valid physical mode exists.

$$\sinh(\alpha a) = 0. \tag{3.76}$$

From equation (3.76), the dispersion relation involving hyperbolic functions is obtained, which describes the relationship between the system parameters and the wave propagation characteristics.

Solving this dispersion relation provides the eigenvalue, representing the allowable propagation constant or frequency for the given mode.

$$\alpha_m = \frac{im\pi}{a}, \quad m = 1, 2, 3, \ldots \tag{3.77}$$

Substituting equation (3.77) into equation (3.73), the eigenfunctions

$$X_{2m}(x) = \sinh\left(\frac{im\pi}{a}x\right), \quad m = 1, 2, 3, \ldots \tag{3.78}$$

Accordingly from equation (3.64), we can write $Y_{2n}(y)$ as

$$\frac{1}{Y_{2n}}\frac{\partial^2 Y_{2n}}{\partial y^2} - \lambda_{mn}^2 + \alpha^2 = 0, \tag{3.79}$$

or

$$\frac{1}{Y_{2n}}\frac{\partial^2 Y_{2n}}{\partial y^2} - \beta^2 = 0, \tag{3.80}$$

where

$$-\beta^2 = -\lambda_{mn}^2 + \alpha^2. \tag{3.81}$$

Now equation (3.80) can be solved to obtain

$$Y_{2n}(y) = c_7 \cosh(\beta y) + c_8 \sinh(\beta y), \tag{3.82}$$

where c_7 and c_8 are arbitrary constants. Under simply supported boundary conditions, we derive the corresponding relations.

$$Y_{2n}(0) = 0, \tag{3.83}$$

$$Y_{2n}(b) = 0, \tag{3.84}$$

$$Y_{2n}^{''}(0) = 0, \tag{3.85}$$

$$Y_{2n}^{''}(b) = 0. \tag{3.86}$$

From equation (3.82) and equation (3.83), we can write

$$Y_{2n}(0) = c_7 \cosh(0) + c_8 \sinh(0) = 0, \tag{3.87}$$

which yield

$$c_7 = 0. \tag{3.88}$$

Substituting $c_7 = 0$ into equation (3.83), we get

$$Y_{2n}(y) = c_8 \sinh(\beta y). \tag{3.89}$$

Taking double derivative of equation equation (3.89), gives

$$Y_{2n}^{''}(y) = -\beta^2 c_8 \sinh(\beta y). \tag{3.90}$$

and equation (3.86), we find

$$Y_{2n}^{''}(b) = -\beta^2 c_8 \sinh(\beta b) = 0, \tag{3.91}$$

which yileds $c_2 \neq 0$ for non trivial solution, therefore

$$\sinh(\beta b) = 0. \tag{3.92}$$

From equation (3.92), we get the dispersion relation of hyperbolic function whose eigenvalue is:

$$\beta_n = \frac{in\pi}{b}, \quad n = 1, 2, 3, \ldots \tag{3.93}$$

Substituting equation (3.93) into equation (3.89), the eigenfunctions

$$Y_{2n}(y) = \sinh\left(\frac{in\pi}{b}y\right), \quad n = 1, 2, 3, \ldots \tag{3.94}$$

$$\phi_{2mn}(x, y) = \sin\left(\frac{in\pi}{b}y\right)\sin\left(\frac{im\pi}{a}x\right). \tag{3.95}$$

Now we assume the harmonic form of the displacement as

$$W(x, y, t) = w(x, y)e^{i\omega t}. \tag{3.96}$$

Projecting the displacement $w(x, y)$ on orthogonal basis we may assume as

$$W(x, y, t) = \sum_{m=1}^{\infty}\sum_{n=1}^{\infty} A_{mn}\sin\left(\frac{m\pi}{a}x\right)\sin\left(\frac{n\pi}{b}y\right)e^{i\omega t}. \tag{3.97}$$

Computing the first four partial derivatives of equation (3.97) with respect to x and y , to compute the value of $\Delta^4 W$.

The differentiation with respect to x yield,

$$\frac{\partial W}{\partial x}(x, y, t) = \sum_{m=1}^{\infty}\sum_{n=1}^{\infty} A_{mn}\left(\frac{m\pi}{a}\right)\cos\left(\frac{m\pi}{a}x\right)\sin\left(\frac{n\pi}{b}y\right)e^{i\omega t}, \tag{3.98}$$

$$\frac{\partial^2 W}{\partial x^2}(x, y, t) = \sum_{m=1}^{\infty}\sum_{n=1}^{\infty} A_{mn}\left(\frac{-m\pi}{a}\right)^2\sin\left(\frac{m\pi}{a}x\right)\sin\left(\frac{n\pi}{b}y\right)e^{i\omega t}, \tag{3.99}$$

$$\frac{\partial^3 W}{\partial x^3}(x, y, t) = \sum_{m=1}^{\infty}\sum_{n=1}^{\infty} A_{mn}\left(\frac{-m\pi}{a}\right)^3\cos\left(\frac{m\pi}{a}x\right)\sin\left(\frac{n\pi}{b}y\right)e^{i\omega t}, \tag{3.100}$$

$$\frac{\partial^4 W}{\partial x^4}(x, y, t) = \sum_{m=1}^{\infty}\sum_{n=1}^{\infty} A_{mn}\left(\frac{m\pi}{a}\right)^4\sin\left(\frac{m\pi}{a}x\right)\sin\left(\frac{n\pi}{b}y\right)e^{i\omega t}. \tag{3.101}$$

Similarly, the differentiation with respect to y leads,

$$\frac{\partial W}{\partial y}(x, y, t) = \sum_{m=1}^{\infty}\sum_{n=1}^{\infty} A_{mn}\left(\frac{n\pi}{b}\right)\sin\left(\frac{m\pi}{a}x\right)\cos\left(\frac{n\pi}{b}y\right)e^{i\omega t}, \tag{3.102}$$

$$\frac{\partial^2 W}{\partial y^2}(x, y, t) = \sum_{m=1}^{\infty}\sum_{n=1}^{\infty} A_{mn}\left(\frac{-n\pi}{b}\right)^2\sin\left(\frac{m\pi}{a}x\right)\sin\left(\frac{n\pi}{b}y\right)e^{i\omega t}, \tag{3.103}$$

$$\frac{\partial^3 W}{\partial y^3}(x,y,t) = \sum_{m=1}^{\infty}\sum_{n=1}^{\infty} A_{mn}\left(\frac{-n\pi}{b}\right)^3 \sin\left(\frac{m\pi}{a}x\right)\cos\left(\frac{n\pi}{b}y\right)e^{i\omega t}, \tag{3.104}$$

$$\frac{\partial^4 W}{\partial y^4}(x,y,t) = \sum_{m=1}^{\infty}\sum_{n=1}^{\infty} A_{mn}\left(\frac{n\pi}{b}\right)^4 \sin\left(\frac{m\pi}{a}x\right)\sin\left(\frac{n\pi}{b}y\right)e^{i\omega t}. \tag{3.105}$$

Now, consider the followin

$$\Delta^4 W = \left(\frac{\partial^4 W}{\partial x^4} + \frac{\partial^4 W}{\partial y^4} + 2\frac{\partial^4 W}{\partial x^2 \partial y^2}\right). \tag{3.106}$$

Using equation (3.99), equation (3.101), equation (3.103) and equation (3.105) in equation (3.106), we get

$$\Delta^4 W = \sum_{m=1}^{\infty}\sum_{n=1}^{\infty} A_{mn}\left(\left(\frac{m\pi}{a}\right)^2\left(\frac{n\pi}{b}\right)^2\right)^2 \sin\left(\frac{m\pi}{a}x\right)\sin\left(\frac{n\pi}{b}y\right)e^{i\omega t}. \tag{3.107}$$

Here $\sin\left(\frac{m\pi}{a}x\right)$, $m = 1,2,3,\ldots$ and $\sin\left(\frac{n\pi}{b}y\right)$, $n = 1,2,3,\ldots$ are orthogonal and satisfies the orthonality relations

$$\int_0^a \sin\left(\frac{m\pi}{a}x\right)\sin\left(\frac{p\pi}{a}x\right)dx = \delta_{mp}E_p, \tag{3.108}$$

and

$$\int_0^b \sin\left(\frac{n\pi}{b}y\right)\sin\left(\frac{q\pi}{b}y\right)dy = \delta_{mq}F_q. \tag{3.109}$$

Velocity is the time derivative of the displacement $W(x,y,t)$:

$$v(x,y,t) = \frac{\partial W}{\partial t}(x,y,t). \tag{3.110}$$

Using the W from equation (3.97), we get

$$v(x,y,t) = \sum_{m=1}^{\infty}\sum_{n=1}^{\infty} i\omega A_{mn}\sin\left(\frac{m\pi}{a}x\right)\sin\left(\frac{n\pi}{b}y\right)e^{i\omega t}, \tag{3.111}$$

or

$$v(x,y,t) = \sum_{m=1}^{\infty}\sum_{n=1}^{\infty} B_{mn}\sin\left(\frac{m\pi}{a}x\right)\sin\left(\frac{n\pi}{b}y\right)e^{i\omega t}, \tag{3.112}$$

where

$$i\omega A_{mn} = B_{mn}. \tag{3.113}$$

Substituting equation (3.112) and equation (3.107) into equation (3.1), we get

$$\sum_{m=1}^{M}\sum_{n=1}^{N} D_p\left(\left(\frac{m\pi}{a}\right)^2+\left(\frac{n\pi}{b}\right)^2\right)^2 A_{mn}\sin\left(\frac{m\pi}{a}x\right)\sin\left(\frac{n\pi}{b}y\right) + \rho_{eff}(\omega)h\sum_{m=1}^{M}\sum_{n=1}^{N} i\omega B_{mn}\sin\left(\frac{m\pi}{a}x\right)\sin\left(\frac{n\pi}{b}y\right) = \Delta\bar{p}. \tag{3.114}$$

Multiplying and dividing equation (3.114), with $\rho_{eff}(\omega)h$, we get

$$\sum_{m=1}^{M}\sum_{n=1}^{N}\sin\left(\frac{m\pi}{a}x\right)\sin\left(\frac{n\pi}{b}y\right)\left(\frac{D_p\left(\left(\frac{m\pi}{a}\right)^2+\left(\frac{n\pi}{b}\right)^2\right)^2}{\rho_{eff}(\omega)h}A_{mn}\rho_{eff}(\omega)h + i\omega B_{mn}\rho_{eff}(\omega)h\right) = \Delta\bar{p}. \tag{3.115}$$

or

$$\sum_{m=1}^{M}\sum_{n=1}^{N}\sin\left(\frac{m\pi}{a}x\right)\sin\left(\frac{n\pi}{b}y\right)(\omega_{mn}^2 A_{mn}\rho_{eff}(\omega)h + i\omega B_{mn}\rho_{eff}(\omega)h) = \Delta\bar{p}, \tag{3.116}$$

where

$$\omega_{mn}^2 = \frac{D_p\left(\left(\frac{m\pi}{a}\right)^2+\left(\frac{n\pi}{b}\right)^2\right)^2}{\rho_{eff}(\omega)h}, \tag{3.117}$$

$$\omega_{mn} = \left(\frac{m\pi}{a}\right)^2+\left(\frac{n\pi}{b}\right)^2\sqrt{\frac{D_P}{\rho_{eff}(\omega)h}}. \tag{3.118}$$

From equation (3.116), we can write:

$$\sum_{m=1}^{M}\sum_{n=1}^{N}\sin\left(\frac{m\pi}{a}x\right)\sin\left(\frac{n\pi}{b}y\right)B_{mn}\left(\frac{\omega_{mn}}{i\omega}+i\omega\right)\rho_{eff}(\omega)h = \Delta\bar{p}, \tag{3.119}$$

or

$$\sum_{m=1}^{M}\sum_{n=1}^{N}\sin\left(\frac{m\pi}{a}x\right)\sin\left(\frac{n\pi}{b}y\right)B_{mn}\left(\frac{\omega_{mn}-\omega^2}{i\omega}\right)\rho_{eff}(\omega)h=\Delta\bar{p}, \tag{3.120}$$

or

$$\sum_{m=1}^{M}\sum_{n=1}^{N}\sin\left(\frac{m\pi}{a}x\right)\sin\left(\frac{n\pi}{b}y\right)B_{mn}(\frac{i}{i})\left(\frac{\omega_{mn}-\omega^2}{i\omega}\right)\rho_{eff}(\omega)h=\Delta\bar{p}, \tag{3.121}$$

or

$$\sum_{m=1}^{M}\sum_{n=1}^{N}\sin\left(\frac{m\pi}{a}x\right)\sin\left(\frac{n\pi}{b}y\right)B_{mn}\left(\frac{\omega^2-\omega_{mn}}{\omega}\right)\rho_{eff}(\omega)hi=\Delta\bar{p}, \tag{3.122}$$

or

$$\sum_{m=1}^{M}\sum_{n=1}^{N}\sin\left(\frac{m\pi}{a}x\right)\sin\left(\frac{n\pi}{b}y\right)B_{mn}Z_{mn}=\Delta\bar{p}, \tag{3.123}$$

where

$$Z_{mn}=\rho_{eff}(\omega)hi\left(\frac{\omega^2-\omega_{mn}}{\omega}\right). \tag{3.124}$$

Structural damping is considered in the host panel, resulting in

$$Z_{mn}=\rho_{eff}(\omega)h\frac{\eta_P\omega_{mn}\omega+i(\omega^2-\omega_{mn}^2)}{\omega}. \tag{3.125}$$

The quantity η_p denotes the damping loss factor of the host panel, while ω_{mn} represents the resonance frequency of the (m,n) mode of (MMPP).

Multiplying equation (3.123), with $\left(\sin\left(\frac{p\pi}{a}x\right)\sin\left(\frac{q\pi}{b}y\right)\right)$ and integrating from $0<x<a$ and $0<y<b$, we obtain

$$\int_0^a\int_0^b\sum_{m=1}^{M}\sum_{n=1}^{N}Z_{mn}B_{mn}\sin\left(\frac{m\pi}{a}x\right)\sin\left(\frac{n\pi}{b}y\right)\sin\left(\frac{p\pi}{a}x\right)\sin\left(\frac{q\pi}{b}y\right)dxdy$$
$$=\Delta\bar{p}\int_0^a\int_0^b\sin\left(\frac{p\pi}{a}x\right)\sin\left(\frac{q\pi}{b}y\right)dxdy, \tag{3.126}$$

or

$$\sum_{m=1}^{M}\sum_{n=1}^{N} Z_{mn}B_{mn}\delta_{mp}E_P\delta_{nq}Fq = \Delta\bar{p}\int_0^a\int_0^b \sin\left(\frac{p\pi}{a}x\right)\sin\left(\frac{q\pi}{b}y\right)dxdy, \quad (3.127)$$

or

$$Z_{mn}B_{mn}E_PFq = \Delta\bar{p}\int_0^a\int_0^b \sin\left(\frac{p\pi}{a}x\right)\sin\left(\frac{q\pi}{b}y\right)dxdy, \quad (3.128)$$

From equation (3.128), we can write

$$B_{mn} = \frac{\Delta\bar{p}}{Z_{mn}E_pF_q}\int_0^a\int_0^b \sin\left(\frac{p\pi}{a}x\right)\sin\left(\frac{q\pi}{b}y\right)dxdy \quad (3.129)$$

The average velocity of the panel frame is obtained as:

$$\bar{v} = \frac{\int_0^a\int_0^b v dxdy}{ab}. \quad (3.130)$$

Substituting equation (3.112) into equation (3.130), we get

$$\bar{v} = \frac{\int_0^a\int_0^b\sum_{m=1}^{M}\sum_{n=1}^{N} B_{mn}\sin\left(\frac{m\pi}{a}x\right)\sin\left(\frac{n\pi}{b}y\right)dxdy}{ab}, \quad (3.131)$$

or

$$\bar{v} = \frac{\sum_{m=1}^{M}\sum_{n=1}^{N} B_{mn}\int_0^a\int_0^b \sin\left(\frac{m\pi}{a}x\right)\sin\left(\frac{n\pi}{b}y\right)dxdy}{ab}. \quad (3.132)$$

Replacing the value of B_{mn} in equation (3.132), we get

$$\bar{v} = \frac{1}{ab}\sum_{m=1}^{M}\sum_{n=1}^{N}\left(\frac{\Delta\bar{p}}{Z_{mn}E_pF_q}\int_0^a\int_0^b \sin\left(\frac{m\pi}{a}x\right)\sin\left(\frac{n\pi}{b}y\right)dxdy\right) \int_0^a\int_0^b \sin\left(\frac{m\pi}{a}x\right)\sin\left(\frac{n\pi}{b}y\right)dxdy, \quad (3.133)$$

or

$$\bar{v} = \Delta\bar{p}\sum_{m=1}^{M}\sum_{n=1}^{N}\frac{\int_0^a\int_0^b \sin^2\left(\frac{m\pi}{a}x\right)\sin^2\left(\frac{n\pi}{b}y\right)dxdy}{abZ_{mn}E_pF_q}. \quad (3.134)$$

From equation (3.134), we can write:

$$\bar{v} = \Delta\bar{p} \sum_{m=1}^{M} \sum_{n=1}^{N} \frac{\epsilon_{mn}^2}{abZ_{mn}E_pF_q}, \tag{3.135}$$

where

$$\epsilon_{mn}^2 = \int_0^a \int_0^b \sin^2\left(\frac{m\pi}{a}x\right) \sin^2\left(\frac{n\pi}{b}y\right) dxdy. \tag{3.136}$$

The panel frame's impedance can be computed as follows:

$$Z = \frac{\Delta\bar{p}}{\bar{v}}, \tag{3.137}$$

the impedance Z of the panel frame of the (MMPP) can also be used to determine $\bar{v}$.

$$Z = \frac{\Delta\bar{p}}{\Delta\bar{p}\left(\sum_{m=1}^{M}\sum_{n=1}^{N} \frac{\epsilon_{mn}^2}{abZ_{mn}E_pF_q}\right)}, \tag{3.138}$$

or

$$Z = \sum_{m=1}^{M} \sum_{n=1}^{N} \left(\frac{\epsilon_{mn}^2}{abZ_{mn}E_pF_q}\right)^{-1}. \tag{3.139}$$

3.2.1 Numerical Solution

The problem is solved analytically using the given formulas after retaining only the first 16 terms of the equations ($N = 16$). These truncated equations are then solved in Mathematica using the "NSolve" function for the case of an Acoustic Impedance of an Elastic Plate in a Rigid Infinite Waveguide. The following numerical values of the parameters are used in the calculations: $c_0 = 343$, $\rho_0 = 1.23$, $\eta = 1.95$, $a = b = 63.5$, $d = 0.8 \times 10^3$, $h = 0.5 \times 10^{-3}$, $\phi = 0.008$, $D_1 = 0.048$, $E_p = 69 \times 10^9$, $\nu_p = 0.33$, $\rho_p = 2730$, $\eta_p = 0.005$, $m_r = 34.4 \times 10^{-6}$, $k_r = 487.13$, $\eta_r = 0.02$, and $N = 16$. The impedance expressions are evaluated over the frequency range of interest and the results plotted for the real and imaginary parts of Z, as well as the absorption coefficient α. The numerical plots indicate that at low frequencies, the impedance is predominantly reactive, while near the resonance frequencies of the elastic plate, the real part of the impedance increases, leading

to higher absorption. The results also show multiple sharp dips in the reflection spectrum, corresponding to the structural resonance modes of the plate.

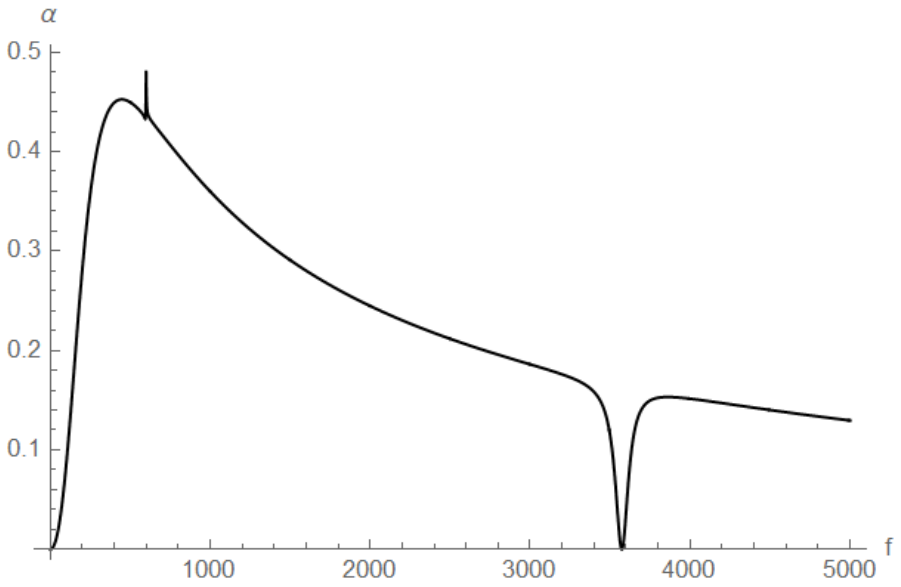

FIGURE 3.2: Graph of sound absorption coefficient α against frequency f

Figure (3.2) shows how the sound absorption coefficient varies with frequency. At lower frequencies, the absorption is relatively high, but it gradually decreases as the frequency increases. A noticeable dip occurs around 3,500 Hz, indicating a point of minimal absorption. The frequency (x-axis) ranges from 0 to 5,000 Hz, while the absorption coefficient (y-axis) ranges from 0 to 0.5.

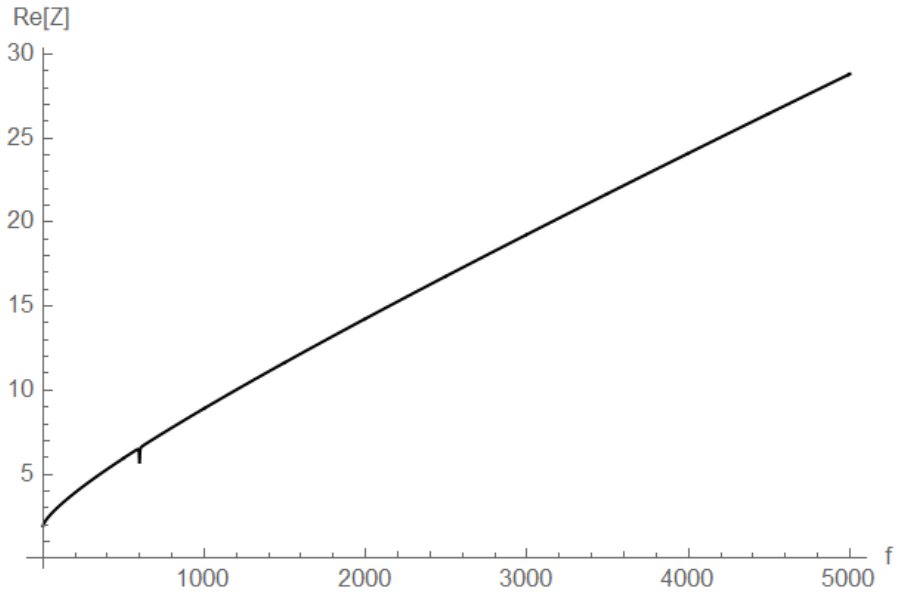

FIGURE 3.3: Graph of real part of impedance Z against frequency f

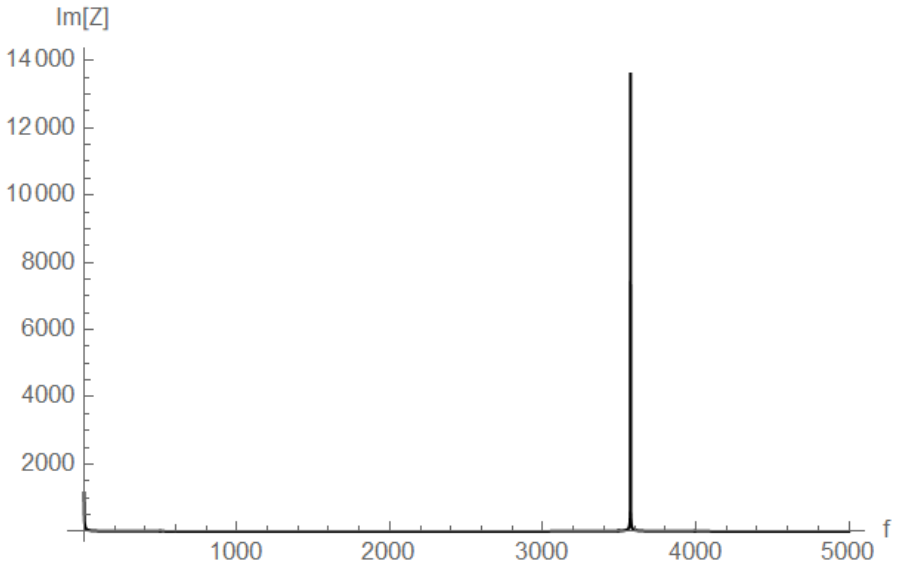

FIGURE 3.4: Graph of imaginary part of impedance Z against frequency f

Figure (3.3) presents the variation of the real part of the acoustic impedance with respect to frequency. As the frequency increases, the real component of the impedance rises consistently, suggesting that sound encounters greater resistance at higher frequencies. The x-axis spans from 0 to 5,000 Hz, and the y-axis ranges from 0 to 30. Figure (3.4) shows how the imaginary part of the impedance changes with frequency for an elastic plate in a rigid waveguide. A clear peak appears at 3,500 Hz, after which the reactance decreases. This helps explain how the plate interacts with sound in the surrounding medium.

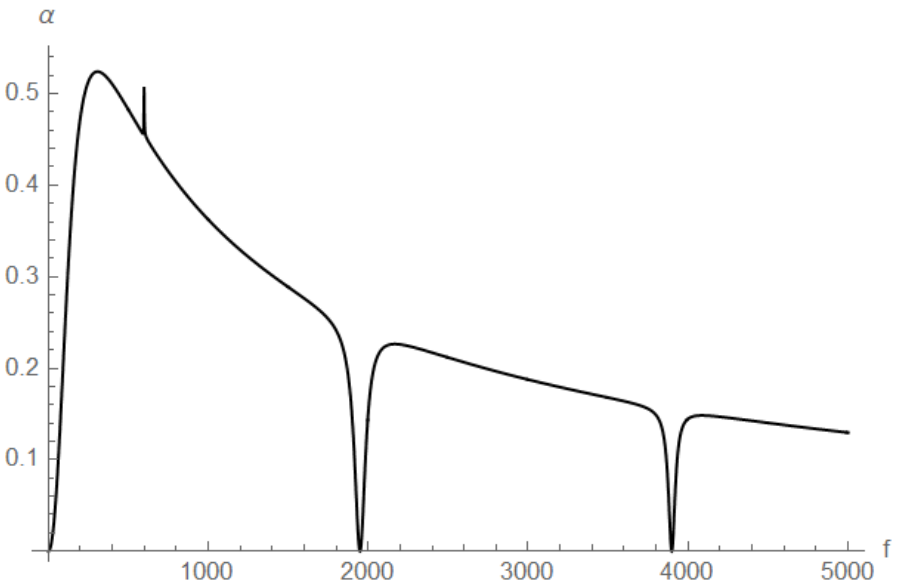

FIGURE 3.5: Graph of sound absorption coefficient α against frequency f

Figure (3.5) shows how the sound absorption α changes with frequency. It dips at 2000 Hz, 4000 Hz, and one more low point is seen before that. At 500 Hz, α is about 0.5.

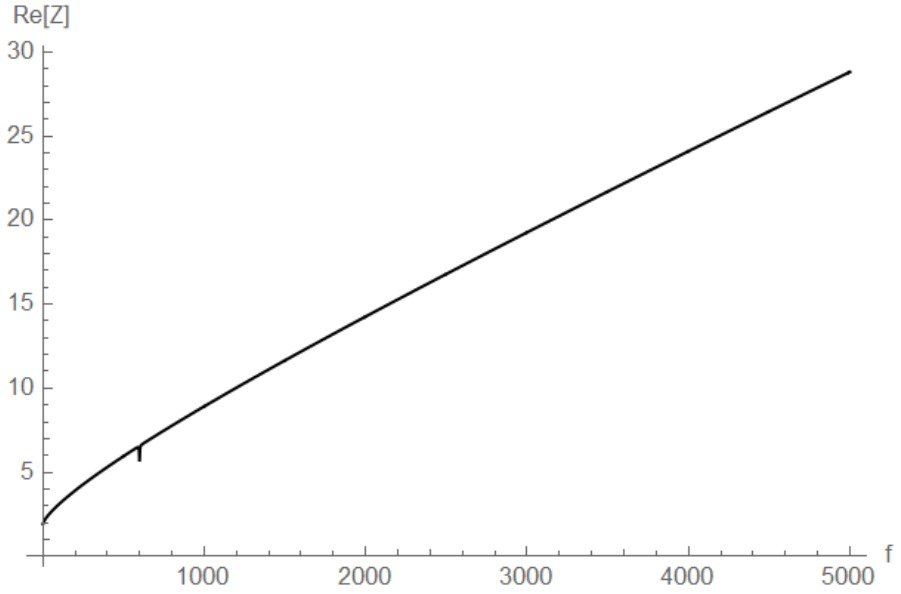

FIGURE 3.6: Graph of real part of impedance Z against frequency f

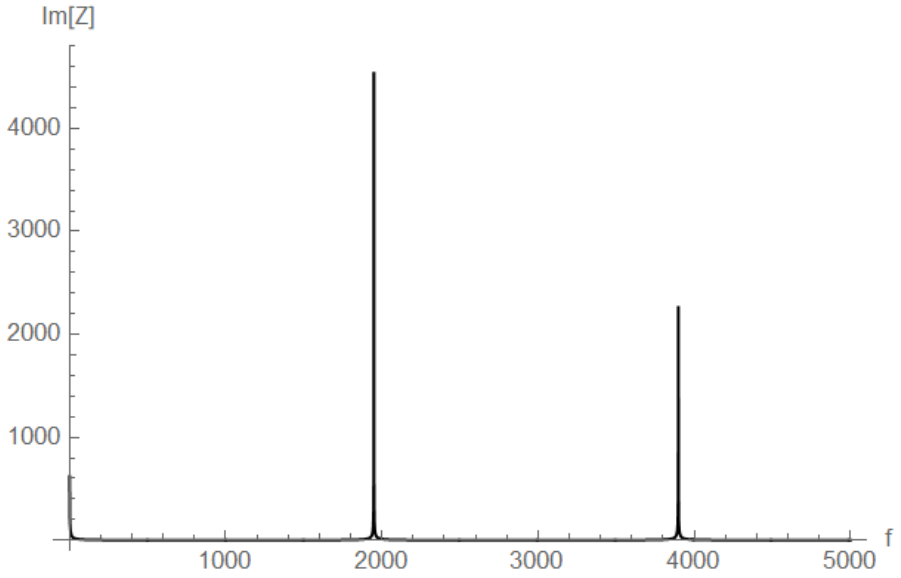

FIGURE 3.7: Graph of imaginary part of impedance Z against frequency f

Figure (3.6) shows as the frequency increases, Re[Z] also increases. The x-axis covers a wide range from 0 to 5000 Hz, and the y-axis goes from 0 to 30. Figure (3.7) shows the imaginary part of impedance, Im[Z], against frequency. The x-axis ranges from 0 to 5000 Hz, and the y-axis from 0 to 4000. There are two sharp

peaks in the graph: one at 2000 Hz reaching about 4500, and another at 4000 Hz around 2000. Outside these points, the graph stays at zero. This suggests that Im[Z] only reacts at specific frequencies, likely due to resonance.

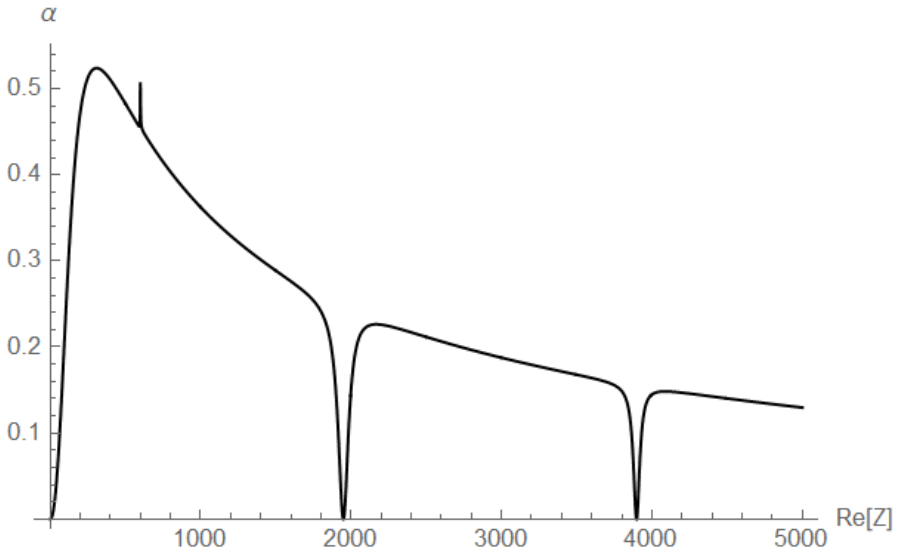

FIGURE 3.8: Graph of sound absorption coefficient α against real part of impedance Z

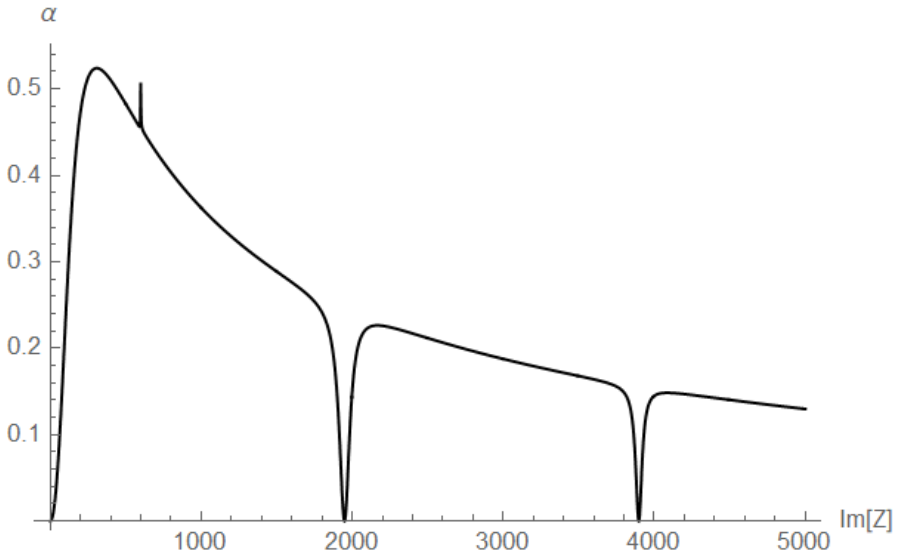

FIGURE 3.9: Graph of sound absorption coefficient α against imaginary part of impedance Z

Figure (3.8) shows the real part of impedance increases, α rises to a peak at 500, then slowly falls. Around 4000, α dips to near zero before slightly rising again. Figure (3.9) shows the behavior at low imaginary impedance, α is high (peak at

500), but decreases as impedance increases. Around 4000, α drops sharply to nearly zero.

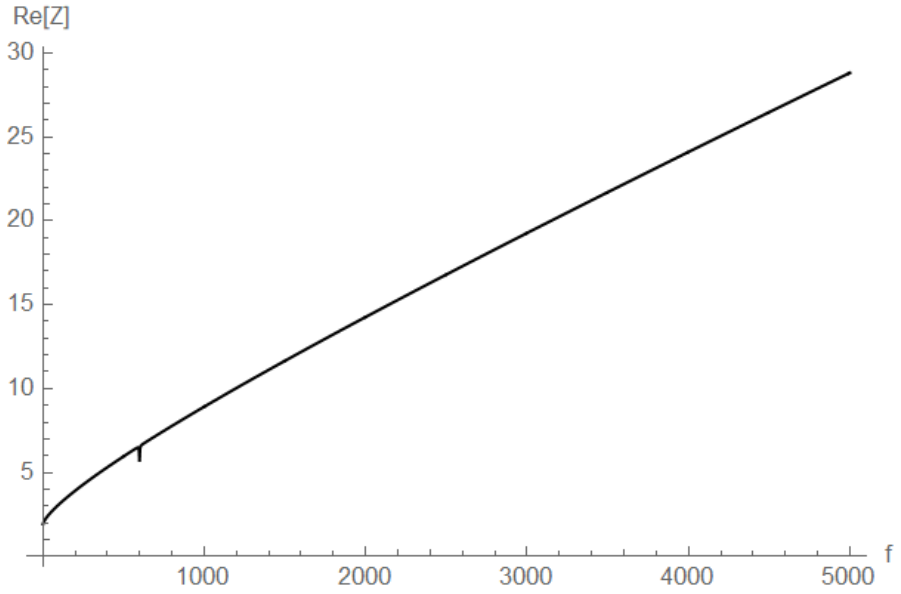

FIGURE 3.10: Graph of real part of impedance Z against frequency f

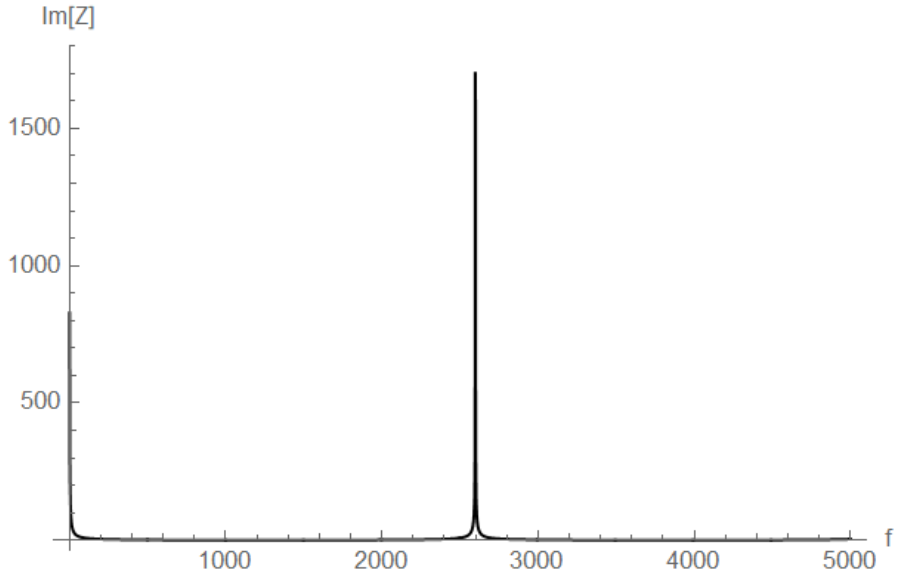

FIGURE 3.11: Graph of imaginary part of impedance Z against frequency f

Figure (3.10) shows that the real part of impedance increases as the frequency increases. The rise is not linear it becomes steeper at higher frequencies, meaning the impedance grows faster with increasing frequency. Figure (3.11) shows two clear peaks in the imaginary part of impedance at specific frequencies.

Chapter 4

Scattering from an Elastic Plate in a 3-Dimensional Rectangular Waveguide

4.1 Introduction

This chapter focuses on the detailed analysis of a simply supported panel frame that incorporates a micro-perforated panel with metamaterial properties (MMPP). The study investigates its harmonic displacement and overall behavior when subjected to structural forces and acoustic loading. The discussion begins with the derivation of the governing equations for displacement in both the and directions, applying the boundary conditions appropriate for a simply supported configuration. These formulations lead to the determination of eigenfunctions and dispersion relations for each direction, ultimately producing the general form of the panel's displacement functions. A harmonic representation of the displacement field is then developed, from which velocity expressions, displacement derivatives, and associated governing relations are obtained. The concept of structural damping is incorporated by introducing a damping factor into the governing equations, allowing for the evaluation of the mechanical impedance of the panel frame. The

analysis also addresses the effect of panel material properties, geometric parameters, and boundary constraints on the dynamic response of the MMPP. Special attention is given to the coupling between the panel's structural modes and the acoustic field inside the surrounding waveguide, emphasizing the role of modal interaction in sound absorption and energy dissipation. Furthermore, the chapter investigates the resonance frequencies, mode shapes, and frequency-dependent impedance behavior of the MMPP. It derives closed-form expressions for average surface velocity, which are essential for computing sound transmission loss and absorption performance. The theoretical developments presented here lay the groundwork for experimental validation, ensuring that the proposed models are practically applicable in real-world acoustic engineering scenarios. The results from this framework also provide valuable guidance for optimizing MMPP designs in practical applications.

4.2 Scattering from a Elastic Plate Backed by Rigid Wall

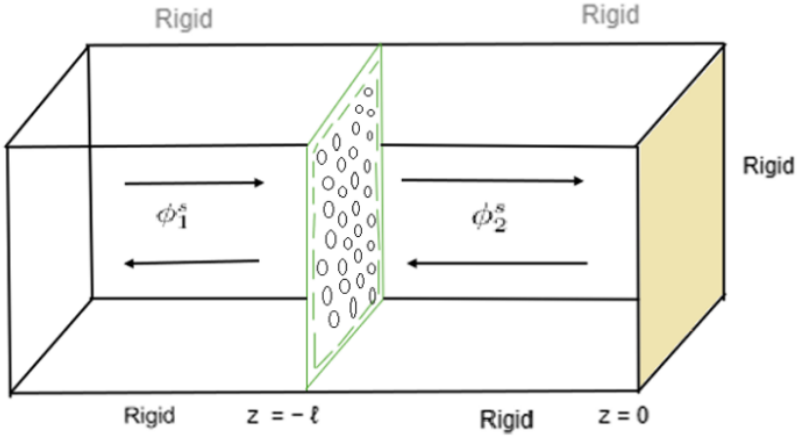

FIGURE 4.1: Physical structure of the waveguide

Consider an elastic plate of dimensions (ab), positioned at $z = -\ell$, with a duct mode. A rigid wall is located at $z = 0$, and the incident mode comes from the region $z < -\ell$. The waveguide geometry is depicted in Figure, (4.1) The compressible fluid inside the waveguide, characterized by density ρ and sound

speed c, satisfies the dimensional wave equation for the fluid potential

$$\left[\frac{\partial^2}{\partial\bar{x}^2}+\frac{\partial^2}{\partial\bar{y}^2}+\frac{\partial^2}{\partial\bar{z}^2}\right]\Phi(\bar{x},\bar{y},\bar{z},\bar{t})=\frac{1}{c^2}\frac{\partial^2\bar{\Phi}}{\partial\bar{t}^2}. \tag{4.1}$$

The fluid potential is connected to the acoustic pressure $\bar{P}$ and velocity vector $\bar{V}$ through the following relationship:

$$\bar{P}=-\rho\frac{\partial\bar{\Phi}}{\partial\bar{t}}, \tag{4.2}$$

and

$$\bar{V}=\bar{\Delta}\bar{\Phi}. \tag{4.3}$$

The boundary condition for the acoustically rigid surface of the waveguide is given by:

$$\frac{\partial\bar{\Phi}}{\partial\bar{x}}=0 \quad at \quad \bar{x}=0,\bar{a} \quad 0\leq\bar{y}\leq\bar{b}, \tag{4.4}$$

$$\frac{\partial\bar{\Phi}}{\partial\bar{y}}=0 \quad at \quad \bar{y}=0,\bar{b} \quad 0\leq\bar{x}\leq\bar{a}. \tag{4.5}$$

A plate exists at $\bar{z}=0$, and the displacement $\bar{W}(\bar{x},\bar{y},\bar{z},\bar{t})$ of this plate satisfies the equation:

$$D_p\bar{\Delta}^4\bar{W}(\bar{x},\bar{y},\bar{t})+\rho_{eff}(\omega)h\frac{\partial^2\bar{W}(\bar{x},\bar{y},\bar{t})}{\partial\bar{t}^2}=(\bar{P}_2-\bar{P}_1). \tag{4.6}$$

The quantities $\bar{P}_1$ and $\bar{P}_2$ on the right-hand side of equation (4.6) represent the acoustic pressures in the regions where $\bar{z}>0$ and $\bar{z}<0$, respectively. Furthermore, boundary conditions are imposed on the edges of the elastic plate. These conditions define the type of physical connection and ensure the uniqueness of the obtained solution. For generality, these simply supported conditions can be expressed as follows:

$$\bar{W}(0,\bar{y},\bar{t})=0, \tag{4.7}$$

$$\bar{W}(a, \bar{y}, \bar{t}) = 0, \tag{4.8}$$

$$\frac{\partial^2 \bar{W}}{d\bar{x}^2}(0, \bar{y}, \bar{t}) = 0, \tag{4.9}$$

$$\frac{\partial^2 \bar{W}}{d\bar{x}^2}(\bar{a}, \bar{y}, \bar{t}) = 0, \tag{4.10}$$

$$\bar{W}(\bar{x}, 0, \bar{t}) = 0, \tag{4.11}$$

$$\bar{W}\bar{x}, \bar{b}, \bar{t}) = 0, \tag{4.12}$$

$$\frac{\partial^2 \bar{W}}{d\bar{y}^2}(\bar{x}, 0, \bar{t}) = 0, \tag{4.13}$$

$$\frac{\partial^2 \bar{W}}{d\bar{y}^2}(\bar{x}, \bar{b}, \bar{t}) = 0. \tag{4.14}$$

The displacement of the plate $\bar{W}$, is linked to the fluid potential $\bar{\Phi}$, through the following relationship:

$$\frac{\partial \bar{W}}{\partial \bar{t}} = \frac{\partial \bar{\Phi}}{\partial \bar{t}}. \tag{4.15}$$

Assuming a harmonic time dependence of the form $e^{i\omega\bar{t}}$, where $\omega = 2\pi f$ represents the radiant frequency, the relationships between $\bar{P}$, $\bar{V}$, $\bar{W}$, and $\bar{\Phi}$ can be expressed as:

$$\bar{P}(\bar{x}, \bar{y}, \bar{z}, \bar{t}) = \bar{p}(\bar{x}, \bar{y}, \bar{z})e^{i\omega\bar{t}}, \tag{4.16}$$

$$\bar{V}(\bar{x}, \bar{y}, \bar{z}, \bar{t}) = \bar{v}(\bar{x}, \bar{y}, \bar{z})e^{i\omega\bar{t}}, \tag{4.17}$$

$$\bar{\Phi}(\bar{x}, \bar{y}, \bar{z}, \bar{t}) = \bar{\phi}(\bar{x}, \bar{y}, \bar{z})e^{i\omega\bar{t}}, \tag{4.18}$$

and

$$\bar{W}(\bar{x}, \bar{y}, \bar{t}) = \bar{w}(\bar{x}, \bar{y})e^{i\omega\bar{t}}. \tag{4.19}$$

Substituting the time-independent variables $\bar{p}, \bar{v}, \bar{w}$ and $\bar{\phi}$ from equation (4.16) to equation (4.19) into equation (4.1) to equation (4.6), we obtain the following equations in terms of harmonic time independent variables

- The Helmholtz's equation

$$\left[\frac{\partial^2}{\partial \bar{x}^2} + \frac{\partial^2}{\partial \bar{y}^2} + \frac{\partial^2}{\partial \bar{z}^2} + k^2\right]\bar{\phi}(\bar{x}, \bar{y}, \bar{z}) = 0. \tag{4.20}$$

- The relationships between pressure, velocity, and displacement with fluid potential can be expressed as:

$$\bar{p}(\bar{x},\bar{y},\bar{z}) = i\omega\rho\bar{\phi}(\bar{x},\bar{y},\bar{z}), \tag{4.21}$$

$$\bar{v}(\bar{x},\bar{y},\bar{z}) = \frac{\partial\bar{\phi}}{\partial\bar{x}}\hat{i} + \frac{\partial\bar{\phi}}{\partial\bar{y}}\hat{j} + \frac{\partial\bar{\phi}}{\partial\bar{z}}\hat{k}, \tag{4.22}$$

$$\bar{w}(\bar{x},\bar{y}) = \frac{i}{\omega}\frac{\partial\bar{\phi}}{\partial\bar{z}}. \tag{4.23}$$

The above equations are non dimensionalized. Using the length scale k^{-1} and the time scale ω^{-1}, the relationship between dimensional variables with bar and non dimensional variables without bar are defined as:

$$\begin{cases} x = k\bar{x}, y = k\bar{y}, z = k\bar{z}, t = \omega\bar{t}, \\ u = k\bar{u}, \phi = \dfrac{k^2}{\omega}\phi. \end{cases} \tag{4.24}$$

The differential operators in the dimensional form are expressed in terms of their non-dimensional counterparts as:

$$\frac{\partial}{\partial\bar{x}} = \frac{\partial}{\partial x}\frac{\partial x}{\partial\bar{x}} = k\frac{\partial}{\partial x}, \tag{4.25}$$

$$\frac{\partial^2}{\partial\bar{x}^2} = \frac{\partial}{\partial\bar{x}}\left(k\frac{\partial}{\partial x}\right) = k^2\frac{\partial^2}{\partial x^2}, \tag{4.26}$$

$$\frac{\partial}{\partial\bar{y}} = \frac{\partial}{\partial y}\frac{\partial y}{\partial\bar{y}} = k\frac{\partial}{\partial y}, \tag{4.27}$$

$$\frac{\partial^2}{\partial\bar{y}^2} = \frac{\partial}{\partial\bar{y}}\left(k\frac{\partial}{\partial y}\right) = k^2\frac{\partial^2}{\partial y^2}, \tag{4.28}$$

$$\frac{\partial}{\partial\bar{z}} = \frac{\partial}{\partial z}\frac{\partial z}{\partial\bar{z}} = k\frac{\partial}{\partial z}, \tag{4.29}$$

$$\frac{\partial^2}{\partial\bar{z}^2} = \frac{\partial}{\partial\bar{z}}\left(k\frac{\partial}{\partial z}\right) = k^2\frac{\partial^2}{\partial z^2}, \tag{4.30}$$

Applying the transformation defined in equation (4.24), we obtain the dimensionless form of the equations as follows:

- The Helmholtz's equation

$$\left[\frac{\partial^2}{\partial x^2}+\frac{\partial^2}{\partial y^2}+\frac{\partial^2}{\partial z^2}+k^2\right]\phi(x,y,z)=0. \tag{4.31}$$

- The relationships between pressure, velocity, and displacement with fluid potential can be expressed as:

$$p(x,y,z)=i\omega\rho\phi(x,y,z), \tag{4.32}$$

$$v(x,y,z)=\frac{\partial\phi}{\partial x}\hat{i}+\frac{\partial\phi}{\partial y}\hat{j}+\frac{\partial\phi}{\partial z}\hat{k}, \tag{4.33}$$

$$w(x,y)=\frac{i}{\omega}\frac{\partial\phi}{\partial z}. \tag{4.34}$$

- Rigid boundary conditions at $x=0,a$ and $y=0,b$.

$$\frac{\partial\Phi}{\partial x}=0 \quad at \quad x=0,a \quad 0\le y\le b, \tag{4.35}$$

$$\frac{\partial\Phi}{\partial y}=0 \quad at \quad y=0,b \quad 0\le x\le a. \tag{4.36}$$

- Elastic plate condition at $z=0, 0\le x\le a, 0\le y\le b$,

$$D_p\Delta^4 W(x,y,t)+\rho_{eff}(\omega)h\frac{\partial^2 W(x,y,t)}{\partial t^2}=\alpha(\phi_2-\phi_1), \tag{4.37}$$

where the dimensionless forms of the elastic plate wavenumber and fluid loading parameters are given by:

$$\alpha=\frac{i\rho\omega}{D_p},$$

and

$$\phi^s(x,y)=\begin{cases}\phi_1^s(x,y) & z<-\ell,\\ \phi_2^s(x,y) & \bar{z}>-\ell.\end{cases} \tag{4.38}$$

The boundary conditions in dimensionless form at the edges of the elastic plate are:

$$W(0, y, t) = 0, \tag{4.39}$$

$$W(a, y, t) = 0, \tag{4.40}$$

$$\frac{\partial^2 W}{dx^2}(0, y, t) = 0, \tag{4.41}$$

$$\frac{\partial^2 W}{d\bar{x}^2}(a, y, t) = 0, \tag{4.42}$$

$$W(x, 0, t) = 0, \tag{4.43}$$

$$W(x, b, t) = 0, \tag{4.44}$$

$$\frac{\partial^2 W}{dy^2}(x, 0, t) = 0, \tag{4.45}$$

$$\frac{\partial^2 W}{d\bar{y}^2}(x, b, t) = 0. \tag{4.46}$$

When an incident wave interacts with the elastic plate, a portion is reflected in region I, while the remaining part is transmitted into region II. To study the reflection and transmission phenomena, we solve the governing boundary value problem (BVP) using the mode-matching technique. The solution is presented in the next section.

4.3 Mode-Matching Solution

This approach begins with the application of the separation of variables method, which enables us to obtain the eigenfunction expansion of the fluid potential in regions I and II of the duct.

$$\phi^s(x, y) = \begin{cases} \phi_1^s(x, y), & z < -\ell, \\ \phi_2^s(x, y), & z > -\ell. \end{cases} \tag{4.47}$$

The superscript 's' denotes symmetric regions that fulfill the Helmholtz equation and rigid boundary conditions.

In region I, the Helmholtz equation is satisfied, which is expressed as:

$$\left[\frac{\partial^2}{\partial x^2}+\frac{\partial^2}{\partial y^2}+\frac{\partial^2}{\partial z^2}+1\right]\phi_1^s(x,y,z)=0, \tag{4.48}$$

subject to the following boundary conditions

$$\frac{\partial \phi_1^s}{\partial x}=0 \quad at \quad x=0,a \quad 0\leq y\leq b, \tag{4.49}$$

$$\frac{\partial \phi_1^s}{\partial y}=0 \quad at \quad y=0,b \quad 0\leq x\leq a. \tag{4.50}$$

Solving equation (4.48) yields an assumed solution:

$$\phi_1^s(x,y,z)=X_1(x)Y_1(y)Z_1(z). \tag{4.51}$$

Substituting equation (4.51) into equation (4.48), and dividing with $X_1(x), Y_1(y), Z_1(z)$,

$$\frac{X_1^{''}(x)}{X_1(x)}+\frac{Y_1^{''}(y)}{Y_1(y)}+\frac{Z_1^{''}(z)}{Z_1(z)}+k^2=0, \tag{4.52}$$

or

$$\frac{X_1^{''}(x)}{X_1(x)}+\frac{Y_1^{''}(y)}{Y_1(y)}+k^2=\frac{Z_1^{''}(z)}{Z_1(z)}=\eta^2. \tag{4.53}$$

The solution of $Z_1(z)$ from equation (4.53) is given by

$$Z_1(z)=c_1e^{i\eta z}+c_2e^{-i\eta z}, \tag{4.54}$$

here c_1 and c_2 represent arbitrary constants. The ordinary differential equation governing $Y_1(y)$ is:

$$\frac{Y_1^{''}(y)}{Y_1(y)}+k^2-\eta^2=0, \tag{4.55}$$

or

$$\frac{Y_1^{''}(y)}{Y_1(y)}+\eta_y^2=0, \tag{4.56}$$

where

$$\eta_y^2=k^2-\eta^2. \tag{4.57}$$

The solution of equation (4.56) is given by:

$$Y_1(y) = c_3 \cos(\eta_y y) + c_4 \sin(\eta_y y), \tag{4.58}$$

where c_3 and c_4 represent arbitrary constants. Combining equation (4.58) and equation (4.50), we can express:

$$Y_1(y) = \cos\left(\frac{n\pi}{b}\right), \tag{4.59}$$

where $\eta_y = \dfrac{n\pi}{b}$ is the eigenvalue obtained from equation (4.58) by applying the boundary conditions, whereas for $X_1(x)$ the ordinary differential equation is

$$\frac{X_1''(x)}{X_1(x)} + \eta_x^2 = 0, \tag{4.60}$$

where

$$\eta^2 = 1 - \eta^2 - \eta_y^2. \tag{4.61}$$

The solution of equation (4.60) is given by:

$$X_1(x) = c_5 \cos(\eta_x x) + c_6 \sin(\eta_x x), \tag{4.62}$$

where c_5 and c_6 represent arbitrary constants. Combining equation (4.62) and equation (4.49), we can express:

$$X_1(x) = \cos\left(\frac{m\pi}{a}\right), \tag{4.63}$$

where $\eta_x = \dfrac{m\pi}{a}$ is the eigenvalue obtained from equation (4.62) by applying the boundary conditions. For supperposition principal, the total field potential in region I, we can write as

$$\phi_1^s(x, y, z) = \sum_{m=0}^{\infty}\sum_{n=0}^{\infty}(A_{mn}^s e^{i\eta_{mn}(z+\ell)} + B_{mn}^s e^{-i\eta_{mn}(z+\ell)})\psi_{mn}(x, y), \tag{4.64}$$

where $\psi_{mn}(x, y)$ represents the eigenfunction in region I, whose value is given by:

$$\psi_{mn}(x,y) = \cos\left(\frac{m\pi}{a}x\right)\cos\left(\frac{n\pi}{b}y\right). \tag{4.65}$$

Here, η_{mn} represents the wave number of the $(mn)^{th}$ mode, as obtained from equation (4.61), and is given by

$$\eta_{mn} = \sqrt{k^2 - \left(\frac{m\pi}{a}\right)^2 - \left(\frac{n\pi}{b}\right)^2}. \tag{4.66}$$

Observe that equation (4.64) decomposes into two terms, where the first term represents the $(mn)^{th}$ mode traveling in the positive direction, and the second term corresponds to the $(mn)^{th}$ mode propagating in the negative z-direction. The coefficients A^s_{mn} and B^s_{mn} quantify the amplitudes of these modes.

The Helmholtz equation for region II can be expressed as:

$$\left[\frac{\partial^2}{\partial x^2} + \frac{\partial^2}{\partial y^2} + \frac{\partial^2}{\partial z^2} + 1\right]\phi^s_2(x,y,z) = 0, \tag{4.67}$$

subject to the following boundary conditions:

$$\frac{\partial \phi^s_2}{\partial x} = 0 \quad at \quad x = 0, a \quad 0 \le y \le b, \tag{4.68}$$

$$\frac{\partial \phi^s_2}{\partial y} = 0 \quad at \quad y = 0, b \quad 0 \le x \le a. \tag{4.69}$$

The solution of equation (4.48) is assumed to be:

$$\phi^s_2(x,y,z) = X_2(x)Y_2(y)Z_2(z). \tag{4.70}$$

Substituting equation (4.70) into equation (4.67), and dividing with $X_2(x), Y_2(y), Z_2(z)$,

$$\frac{X_2''(x)}{X_2(x)} + \frac{Y_2''(y)}{Y_2(y)} + \frac{Z_2''(z)}{Z_2(z)} + k^2 = 0, \tag{4.71}$$

or

$$\frac{X_2''(x)}{X_2(x)} + \frac{Y_2''(y)}{Y_2(y)} + k^2 = \frac{Z_2''(z)}{Z_2(z)} = \eta^2. \tag{4.72}$$

From equation (4.72), the solution of $Z_2(z)$ is

$$Z_2(z) = c_7 e^{i\eta z} + c_8 e^{-i\eta z}, \tag{4.73}$$

where c_7 and c_8 represent arbitrary constants. $Y_2(y)$ satisfies the following ordinary differential equation:

$$\frac{Y_2''(y)}{Y_2(y)} + k^2 - \eta^2 = 0, \tag{4.74}$$

$$\frac{Y_2''(y)}{Y_2(y)} + \eta_y^2 = 0, \tag{4.75}$$

where

$$\eta_y^2 = k^2 - \eta^2. \tag{4.76}$$

The solution of equation (4.75) is given by:

$$Y_2(y) = c_9 \cos(\eta_y y) + c_{10} \sin(\eta_y y), \tag{4.77}$$

here c_9 and c_{10} represent arbitrary constants. From equation (4.77) and equation (4.69)

$$Y_2(y) = \cos\left(\frac{n\pi}{b}\right), \tag{4.78}$$

where $\eta_y = \dfrac{n\pi}{b}$ is the eigenvalue obtained from equation (4.77) by applying the boundary conditions. Whereas, for $X_2(x)$ the ordinary differential equation is

$$\frac{X_2''(x)}{X_2(x)} + \eta_x^2 = 0, \tag{4.79}$$

where

$$\eta^2 = 1 - \eta^2 - \eta_y^2. \tag{4.80}$$

The solution of equation (4.79) is given by

$$X_2(x) = c_{11} \cos(\eta_x x) + c_{12} \sin(\eta_x x), \tag{4.81}$$

where c_{11} and c_{12} represent arbitrary constants.

From equation (4.81) and equation (4.68),

$$X_2(x) = \cos\left(\frac{m\pi}{a}\right), \tag{4.82}$$

where $\eta_x = \dfrac{m\pi}{a}$ is the eigenvalue obtained from equation (4.82) by applying the boundary conditions. For supperposition principle, the total field potential in region II, we can write as

$$\phi_2^s(x,y,z) = \sum_{m=0}^{\infty}\sum_{n=0}^{\infty}(C_{mn}^s e^{i\eta_{mn}z} + D_{mn}^s e^{-i\eta_{mn}z})\psi_{mn}(x,y), \tag{4.83}$$

the eigenfunction in region I is represented by $\psi_{mn}(x,y)$, with its value expressed as

$$\psi_{mn}(x,y) = \cos\left(\frac{m\pi}{a}x\right)\cos\left(\frac{n\pi}{b}y\right). \tag{4.84}$$

Here, η_{mn} represents the wave number of the $(mn)^{th}$ mode, as obtained from equation (4.80), with a value of

$$\eta_{mn} = \sqrt{1 - \left(\frac{m\pi}{a}\right)^2 - \left(\frac{n\pi}{b}\right)^2}. \tag{4.85}$$

It is important to note that $A_{mn}^s, B_{mn}^s, C_{mn}^s$, and D_{mn}^s are unknown coefficients. Assuming a fundamental duct mode with unit amplitude propagating from region II in the positive z-direction, we consider only transmission in region II by setting $D_{mn}^s = 0$ in equation (4.83). Consequently, the expressions equation (4.64) and equation (4.83) become:

$$\phi_1^s(x,y,z) = \sum_{m=0}^{\infty}\sum_{n=0}^{\infty}(A_{mn}^s e^{i\eta_{mn}(z+\ell)} + B_{mn}^s e^{-i\eta_{mn}(z+\ell)})\psi_{mn}(x,y), \tag{4.86}$$

and

$$\phi_2^s(x,y,z) = \sum_{m=0}^{\infty}\sum_{n=0}^{\infty}(C_{mn}^s e^{i\eta_{mn}z} + D_{mn}^s e^{-i\eta_{mn}z})\psi_{mn}(x,y). \tag{4.87}$$

At $z = 0$, the rigid wall leads to

$$\frac{\partial\phi_2^s}{\partial z} = 0, \quad z = 0. \tag{4.88}$$

Substituting equation (4.87) into equation (4.88), we obtain

$$\phi_2^s(x,y,z) = \sum_{m=0}^{\infty}\sum_{n=0}^{\infty}(C_{mn}^s - D_{mn}^s)\psi_{mn}(x,y), \tag{4.89}$$

Simplifying this expression yields

$$C_{mn}^s = D_{mn}^s. \tag{4.90}$$

Substituting the value of D_{mn}^s from equation (4.90) into equation (4.89) gives

$$\phi_2^s(x,y,z) = \sum_{m=0}^{\infty}\sum_{n=0}^{\infty}(2C_{mn}^s\cos(\eta_{mn}z)\psi_{mn}(x,y). \tag{4.91}$$

Once the excitation coefficient A_{mn}^s is specified for duct mode excitation, the coefficients C_{mn}^s and B_{mn}^s become the unknown quantities.
The dynamics of the membrane located at $z = -\ell$ are then examined using the Galerkin method, which allows us to solve for the unknown amplitudes.

4.4 Galerkin Formulation for Elastic Plate Dynamics

The dynamical response of plate at interface $z = -\ell$ in harmonic time dependence

$$D_p\Delta^4 w^s(x,y) - \rho_{eff}h\omega^2 w^s(x,y) = (\phi_1^s - \phi_2^s)i\rho\omega. \tag{4.92}$$

or

$$\Delta^4 w^s - \mu^4 w^s = \alpha(\phi_1^s - \phi_2^s), \tag{4.93}$$

where

$$\mu = \frac{\rho_{eff}\omega^2 h}{D_p}, \tag{4.94}$$

and

$$\alpha = \frac{i\omega\rho}{D_p}. \tag{4.95}$$

and α are structure wave numberand and thrid loding paramrter

$$w^s(x,y)e^{i\omega t} = 0, \tag{4.96}$$

By applying the appropriate boundary condition, which specifies the physical constraints at the interface, the governing equations can be simplified and solved in a consistent manner.

$$w^s(0,y) = 0, \tag{4.97}$$

$$w^s(a,y) = 0, \tag{4.98}$$

$$\frac{\partial^2 w^s}{dx^2}(0,y) = 0, \tag{4.99}$$

$$\frac{\partial^2 w^s}{dx^2}(a,y) = 0, \tag{4.100}$$

$$w^s(x,0) = 0, \tag{4.101}$$

$$w^s(x,b) = 0, \tag{4.102}$$

$$\frac{\partial^2 w^s}{dy^2}(x,0) = 0, \tag{4.103}$$

$$\frac{\partial^2 w^s}{dy^2}(x,b) = 0. \tag{4.104}$$

Now we can construct the eigenvalue problem associated with equation (4.93) to equation (4.104), given as follows

$$(\Delta^4 - \lambda_{mn}^4)\phi_{mn}^s = 0, \tag{4.105}$$

$$\phi_{mn}^s(0,y) = 0, \tag{4.106}$$

$$\phi_{mn}^s(a,y) = 0, \tag{4.107}$$

$$\phi^{s\prime\prime}{}_{mn}(0,y) = 0, \tag{4.108}$$

$$\phi^{s\prime\prime}{}_{mn}(a,y) = 0, \tag{4.109}$$

$$\phi_{mn}^s(x,0) = 0, \tag{4.110}$$

$$\phi_{mn}^s(x,b) = 0, \tag{4.111}$$

$$\phi^{s\prime\prime}{}_{mn}(x,0) = 0, \tag{4.112}$$

$$\phi^{s\prime\prime}{}_{mn}(x,b) = 0. \tag{4.113}$$

Solution of equation (4.105) to equation (4.113) is as given below

$$\phi^s_{mn}(x,y) = \sin\left(\frac{m\pi}{a}x\right)\sin\left(\frac{n\pi}{b}y\right), \tag{4.114}$$

where

$$\lambda^2_{mn} = \left(\frac{m\pi}{a}\right)^2 + \left(\frac{n\pi}{b}\right)^2 \quad m = 1,2,3\ldots \quad n = 1,2,3\ldots \tag{4.115}$$

The function ϕ^s_{1mn} are orthogonal and satisfies orthogonality relation,

$$\int_0^a \int_0^b \phi^s_{1mn}\phi^s_{1pq}dxdy = E_p\delta_{mp}F_q\delta_{nq}. \tag{4.116}$$

Now we project the solution on orthogonal basis as

$$w^s(x,y) = \sum_{m=1}^{\infty}\sum_{n=1}^{\infty} g^s_{mn}\phi^s_{mn}. \tag{4.117}$$

Using the value of equation (4.117), equation (4.86), equation (4.91) into equation (4.93) we get

$$\sum_{m=1}^{\infty}\sum_{n=1}^{\infty}(\lambda^4_{mn} - \mu^4)g^s_{mn}\phi^s_{mn} = \alpha\sum_{m=1}^{\infty}\sum_{n=1}^{\infty}(A^s_{mn} + B^s_{mn} - 2C^s_{mn}\cos(\eta_{mn}z))\psi_{mn}(x,y), \tag{4.118}$$

Multiplying with ϕ^s_{pq} and integrating from $0 < x < a$ and $0 < y < b$ we may get

$$g^s_{pq} = \frac{\alpha}{(\lambda^4_{pq} - \mu^4)E_pF_q}\sum_{m=1}^{\infty}\sum_{n=1}^{\infty}(A^s_{pq} + B^s_{pq} - 2C^s_{mn}\cos(\eta_{pq}z))\Delta_{pq}, \tag{4.119}$$

where

$$\Delta_{pq} = \int_0^a \int_0^b \phi^s_{pq}\psi_{pq}(x,y). \tag{4.120}$$

At $z = -\ell$ for the coefficients of region I,

$$\frac{\partial \phi_1^s}{\partial z} = w^s(x, y). \tag{4.121}$$

Using equation (4.86) and equation (4.117) into equation (4.121) we get

$$i \sum_{m=0}^{\infty} \sum_{n=0}^{\infty} (A_{mn}^s - B_{mn}^s) \eta_{mn} \psi_{mn}(x, y) = \sum_{m=0}^{\infty} \sum_{n=0}^{\infty} g_{mn}^s \phi_{mn}^s. \tag{4.122}$$

Multiplying with ψ_{1pq}^s and integrating from $0 < x < a$ and $0 < y < b$ we may get

$$A_{pq}^s - B_{pq}^s = \frac{1}{i \eta_{pq} E_p F_q} \sum_{m=0}^{\infty} \sum_{n=0}^{\infty} g_{pq}^s \int_0^a \int_0^b \phi_{1pq}^s \psi_{1pq}^s dx dy, \tag{4.123}$$

or

$$A_{pq}^s - B_{pq}^s = \frac{1}{i \eta_{pq} E_p F_q} \sum_{m=0}^{\infty} \sum_{n=0}^{\infty} g_{pq}^s \Delta_{pq}, \tag{4.124}$$

where

$$\Delta_{pq} = \int_0^a \int_0^b \phi_{1pq}^s \psi_{pq}^s(x, y). \tag{4.125}$$

Likewise, for the coefficient of region II,at $z = -\ell$

$$\frac{\partial \phi_2^s}{\partial z} = w^s(x, y). \tag{4.126}$$

Using equation (4.91) and equation (4.117) into equation (4.126) we get

$$\sum_{m=0}^{\infty} \sum_{n=0}^{\infty} 2 C_{mn}^s \eta_m n \sin(\eta_{mn\ell}) \psi_{mn}(x, y) = \sum_{m=0}^{\infty} \sum_{n=0}^{\infty} g_{mn}^s \phi_{mn}^s. \tag{4.127}$$

Multiplying with ψ_{2pq}^s and integrating from $0 < x < a$ and $0 < y < b$,

$$C_{pq}^s = \frac{1}{2 \sin \eta_{pq} E_p F_q} \sum_{m=0}^{\infty} \sum_{n=0}^{\infty} g_{pq}^s \int_0^a \int_0^b \phi_{2pq}^s \psi_{2pq}^s dx dy, \tag{4.128}$$

or

$$C_{pq}^s = \frac{1}{2 \sin \eta_{pq} E_p F_q} \sum_{m=0}^{\infty} \sum_{n=0}^{\infty} g_{pq}^s \epsilon_{pq}, \tag{4.129}$$

where

$$\epsilon_{pq} = \int_0^a \int_0^b \phi^s_{1pq} \psi^s_{pq}(x, y). \tag{4.130}$$

4.4.1 Numerical Solution

For the rigid wall-backed plate configuration, the governing equations from Section 4.4 are solved in *Mathematica* with $N = 16$ modal terms retained in the series expansion. The parameters used in the computation are $a = 4000$, $b = 6000$, $L = 2000$, $\rho_0 = 1.23$, and $c_0 = 343$. The mode-matching and Galerkin formulations are applied to evaluate the dimensionless normal velocities and pressures in both acoustic regions. The results indicate that under rigid termination, the velocity amplitudes at $z = -\ell$ remain small for most frequencies, except at the resonance frequencies of the plate. Since the downstream wall is perfectly reflecting, a large portion of the incident acoustic energy is returned, producing a high pressure field near the plate. The resonance peaks appear sharp and narrow, reflecting the low damping and the limited bandwidth of absorption in this configuration.

Moreover, the numerical simulations emphasize the significant role of structural resonance in shaping the acoustic response. When the excitation frequency coincides with a natural mode of the plate, a pronounced amplification in both pressure and velocity is observed at the interface.Away from resonance, however, the system behaves as a highly reflective boundary with negligible energy dissipation.

This behavior confirms that the rigid wall-backed plate acts as a frequency-selective system, where strong coupling between the acoustic field and the plate occurs only in the vicinity of resonance frequencies.
Figure (4.2) displays the real parts of the dimensionless normal velocities $\phi^s_{1z}(x, y, z)$ and $\phi^s_{2z}(x, y, z)$ plotted over x and y at $z = -\ell$. Both components show similar patterns, which agrees with the expected continuity of normal velocities at $z = -\ell$ Figure (4.3) shows the imaginary parts of the same velocities over x and y at $z = -\ell$. Again, the two components behave consistently, supporting the continuity condition at that position.

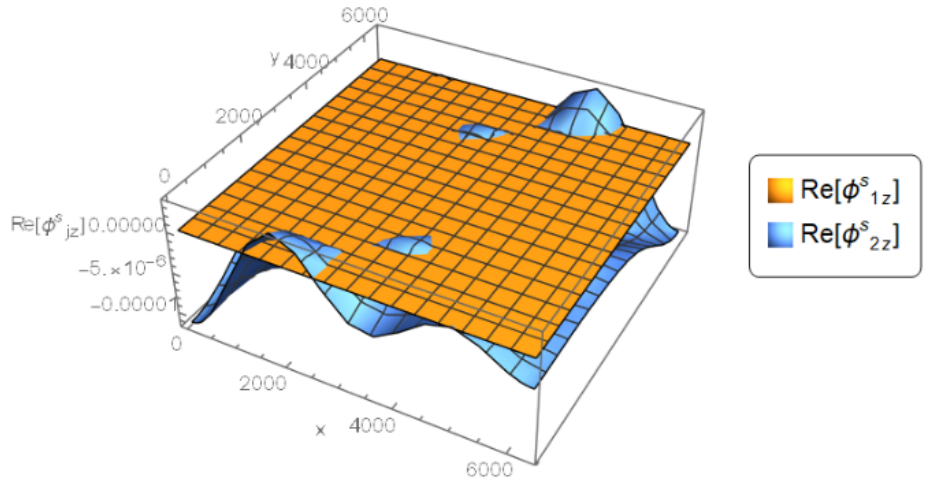

FIGURE 4.2: The real component of dimensionless normal velocities $\phi_1^s(x, y, z)$ and $\phi_2^s(x, y, z)$ against x and y at z=$-\ell$, where $\bar{a} = 4000, \bar{b} = 6000, \bar{L} = 2000$ and N =16 term (Symmetric case)

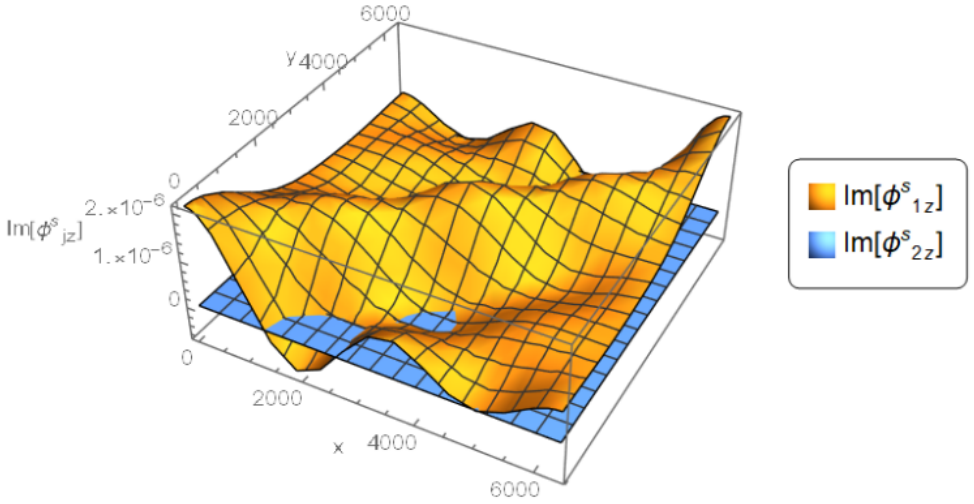

FIGURE 4.3: The imaginary component of dimensionless normal velocities $\phi_1^s(x, y, z)$ and $\phi_2^s(x, y, z)$ against x and y at z=$-\ell$, where $\bar{a} = 4000, \bar{b} = 6000, \bar{L} = 2000$ and N =16 term (Symmetric case)

As shown in Figure (4.4), it exhibits a clear reflection, indicating that the incident wave is reflected back upon encountering the rigid surface. This reflection suggests that the pressure field exerts a force on the elastic plate situated at the interfaces, causing it to vibrate. The interaction between the incident and reflected pressure fields at the wall plays a crucial role in determining the overall wave dynamics

within the cavity, influencing both the pressure distribution and the elastic plate's vibrational response.

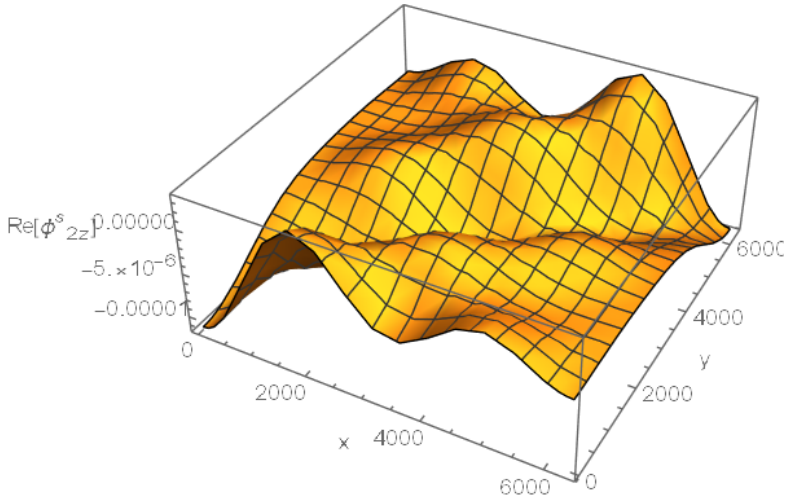

FIGURE 4.4: The real component of dimensionless normal velocity $\phi_2^s(x, y, z)$ against x and y at z=$-\ell$, where $\bar{a} = 4000, \bar{b} = 6000, \bar{L} = 2000$ and N =16 term (Symmetric case)

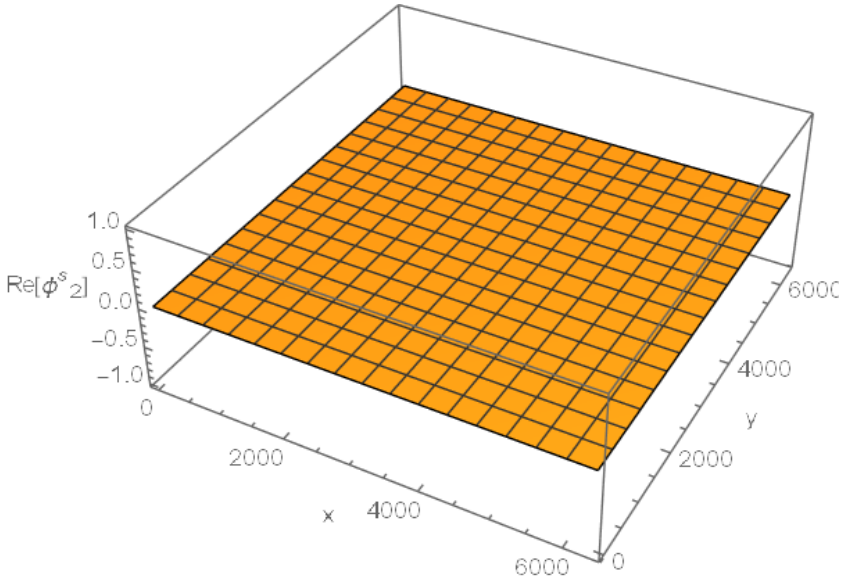

FIGURE 4.5: The real component of dimensionless pressure $\phi_2^s(x, y, z)$ against x and y at z=0, where $\bar{a} = 4000, \bar{b} = 6000, \bar{L} = 2000$ and N =16 term (Symmetric case)

Figure (4.5) shows that at the rigid wall, the velocity is zero, which is consistent with the imposed boundary condition. This result is physically expected, as a rigid boundary should prevent normal motion of the wave at the wall. In contrast, the symmetric pressure field does not vanish at the wall

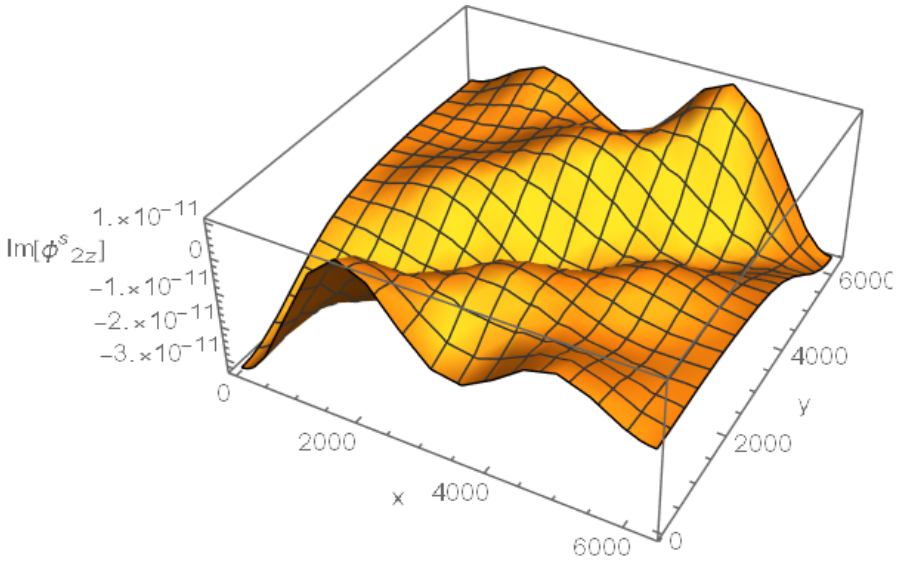

FIGURE 4.6: The imaginary component of dimensionless normal velocity $\phi^s_2(x, y, z)$ against x and y at z=$-\ell$, where $\bar{a} = 4000, \bar{b} = 6000, \bar{L} = 2000$ and N =16 term (Symmetric case)

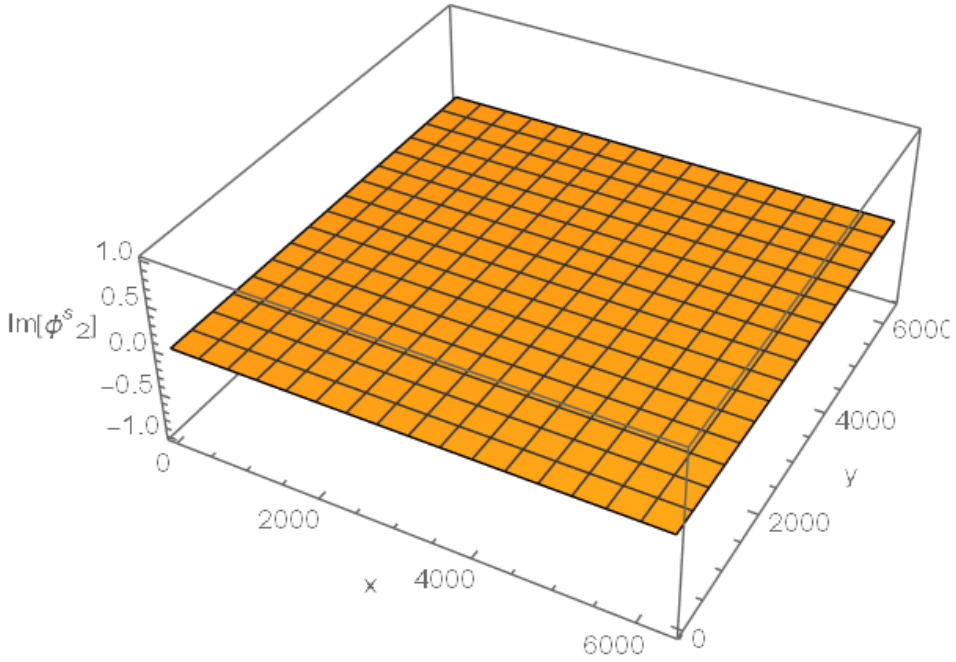

FIGURE 4.7: The imaginary component of dimensionless pressure $\phi^s_2(x, y, z)$ against x and y at z=0, where $\bar{a} = 4000, \bar{b} = 6000, \bar{L} = 2000$ and N =16 term (Symmetric case)

Figure (4.6) shows that the pressure at the wall is not zero. The reflected pressure wave is clearly visible, showing that the incoming wave bounces back from the rigid wall. This reflected wave pushes against the elastic plate at the interface, causing it to vibrate. The interaction between the incoming and reflected waves

affects the overall pressure pattern and how the membrane moves. Figure (4.7) shows that the velocity at the wall is zero, which matches the boundary condition for a rigid surface. This means the wall does not allow any wave motion through it.

4.5 Scattering from a Rectangular Plate Backed by Soft Wall

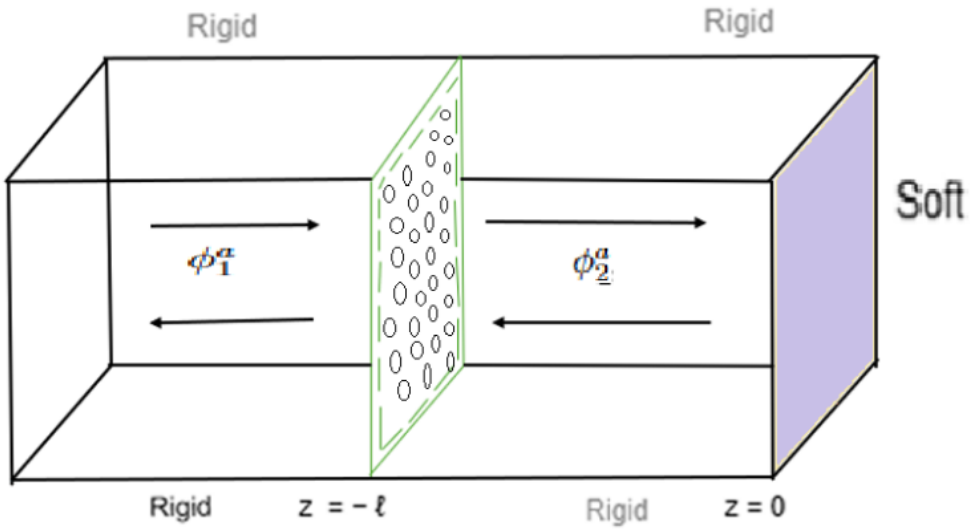

FIGURE 4.8: Physical structure of the waveguide

In this problem, a rectangular duct contains an elastic plate of width a and height b, matching the duct's cross-section, and placed at $z = -\ell$. A rigid wall is located at $z = 0$, which completely reflects incoming acoustic waves. An acoustic mode travels from the upstream region ($z < -\ell$) towards the plate and excites harmonic vibrations.

Part of the incident wave is reflected back upstream, while the rest is either transmitted through or absorbed by the plate. The transmitted wave reflects from the rigid wall, resulting in multiple reflections and standing waves forming between the plate and the wall. The simply supported plate edges together with the rigid wall determine the mode shapes and the dispersion relations. The geometry of the

duct and the wave motion is illustrated in the figure. (4.8) In this configuration, the interaction between the acoustic field and the vibrating plate plays a key role in defining how energy is distributed between reflection, transmission, and absorption. This makes the setup a useful model for studying vibroacoustic coupling and for evaluating how boundary conditions affect wave propagation in ducts and waveguides.

4.6 Mode-Matching Solution

This approach begins with the application of the separation of variables method, which enables us to obtain the eigenfunction expansion of the fluid potential in regions I and II of the duct.

$$\phi^a(x,y) = \begin{cases} \phi_1^a(x,y), & z < -\ell \\ \phi_2^a(x,y), & z > -\ell, \end{cases} \tag{4.131}$$

the superscript 'a' denotes antisymmetric regions that fulfill the Helmholtz equation and rigid boundary condition requirements. For region I, the Helmholtz equation is expressed as:

$$\left[\frac{\partial^2}{\partial x^2} + \frac{\partial^2}{\partial y^2} + \frac{\partial^2}{\partial z^2} + k^2\right]\phi_1^a(x,y,z) = 0, \tag{4.132}$$

subject to the following boundary conditions:

$$\frac{\partial \phi_1^a}{\partial x} = 0 \quad at \quad x = 0, a \quad 0 \le y \le b, \tag{4.133}$$

$$\frac{\partial \phi_1^a}{\partial y} = 0 \quad at \quad y = 0, b \quad 0 \le x \le a. \tag{4.134}$$

We assume a solution of equation(4.132) as follows

$$\phi_1^a(x,y,z) = X_1(x)Y_1(y)Z_1(z). \tag{4.135}$$

Substituting equation (4.135) into equation (4.132), and dividing with $X_1(x), Y_1(y), Z_1(z)$ we get

$$\frac{X_1''(x)}{X_1(x)} + \frac{Y_1''(y)}{Y_1(y)} + \frac{Z_1''(z)}{Z_1(z)} + k^2 = 0, \tag{4.136}$$

or

$$\frac{X_1''(x)}{X_1(x)} + \frac{Y_1''(y)}{Y_1(y)} + k^2 = \frac{Z_1''(z)}{Z_1(z)} = \eta^2. \tag{4.137}$$

The solution for $Z_1(z)$ is derived from equation (4.137) as

$$Z_1(z) = c_1 e^{i\eta z} + c_2 e^{-i\eta z}, \tag{4.138}$$

where c_1 and c_2 denote arbitrary constants. For $Y_1(y)$, we have the following ordinary differential equation

$$\frac{Y_1''(y)}{Y_1(y)} + k^2 - \eta^2 = 0, \tag{4.139}$$

or

$$\frac{Y_1''(y)}{Y_1(y)} + \eta_y^2 = 0, \tag{4.140}$$

where

$$\eta_y^2 = k^2 - \eta^2. \tag{4.141}$$

The solution to equation (4.140) is given by

$$Y_1(y) = c_3 \cos(\eta_y y) + c_4 \sin(\eta_y y), \tag{4.142}$$

here c_3 and c_4 representing arbitrary constants, From equation (4.134) and equation (4.142),

$$Y_1(y) = \cos\left(\frac{n\pi}{b}\right), \tag{4.143}$$

where $\eta_y = \dfrac{n\pi}{b}$ is the eigenvalue obtained from equation (4.142) by applying the boundary conditions, whereas, for $X_1(x)$ the ordinary differential equation is

$$\frac{X_1''(x)}{X_1(x)} + \eta_x^2 = 0, \tag{4.144}$$

where

$$\eta^2 = k^2 - \eta^2 - \eta_y^2. \tag{4.145}$$

The solution to equation (4.144) is given by

$$X_1(x) = c_5 \cos(\eta_x x) + c_6 \sin(\eta_x x), \tag{4.146}$$

where c_5 and c_6 denote arbitrary constants. Combining equation (4.133) and equation (4.146), we can express

$$X_1(x) = \cos\left(\frac{m\pi}{a}\right), \tag{4.147}$$

where $\eta_x = \dfrac{m\pi}{a}$ is the eigenvalue obtained from equation (4.147) by applying the boundary conditions. For supperposition principal, the total field potential in region I, we can write as

$$\phi_1^a(x, y, z) = \sum_{m=0}^{\infty}\sum_{n=0}^{\infty}(A_{mn}^a e^{i\eta_{mn}(z+\ell)} + B_{mn}^a e^{-i\eta_{mn}(z+\ell)})\psi_{mn}(x, y), \tag{4.148}$$

where $\psi_{mn}(x, y)$ represents the eigenfunction in region I, given by

$$\psi_{mn}(x, y) = \cos\left(\frac{m\pi}{a}x\right)\cos\left(\frac{n\pi}{b}y\right). \tag{4.149}$$

where η_{mn} represents the wave number of the $(mn)^{th}$ mode, obtained from equation (4.144), and is given by

$$\eta_{mn} = \sqrt{k^2 - \left(\frac{m\pi}{a}\right)^2 - \left(\frac{n\pi}{b}\right)^2}. \tag{4.150}$$

Observe that equation (4.148) decomposes into two terms, where the first term represents the $(mn)^{th}$ mode traveling in the positive direction, and the second term corresponds to the $(mn)^{th}$ mode propagating in the negative z-direction. The coefficients A_{mn}^a and B_{mn}^a quantify the amplitudes of these modes. The Helmholtz equation for region II is expressed as

$$\left[\frac{\partial^2}{\partial x^2} + \frac{\partial^2}{\partial y^2} + \frac{\partial^2}{\partial z^2} + k^2\right]\phi_2^a(x, y, z) = 0, \tag{4.151}$$

subject to the following boundary conditions:

$$\frac{\partial \phi_2^a}{\partial x} = 0 \quad at \quad x = 0, a \quad 0 \leq y \leq b, \tag{4.152}$$

$$\frac{\partial \phi_2^a}{\partial y} = 0 \quad at \quad y = 0, b \quad 0 \leq x \leq a. \tag{4.153}$$

We assume a solution to equation (4.151) of the form

$$\phi_2^a(x, y, z) = X_2(x)Y_2(y)Z_2(z). \tag{4.154}$$

Substuting equation (4.154) into equation (4.151), and dividing with $X_2(x), Y_2(y), Z_2(z)$ we get

$$\frac{X_2''(x)}{X_2(x)} + \frac{Y_2''(y)}{Y_2(y)} + \frac{Z_2''(z)}{Z_2(z)} + k^2 = 0, \tag{4.155}$$

or

$$\frac{X_2''(x)}{X_2(x)} + \frac{Y_2''(y)}{Y_2(y)} + k^2 = \frac{Z_2''(z)}{Z_2(z)} = \eta^2. \tag{4.156}$$

The solution to $Z_2(z)$, as obtained from equation (4.6), is

$$Z_2(z) = c_7 e^{i\eta z} + c_8 e^{-i\eta z}, \tag{4.157}$$

where c_7 and c_8 denote arbitrary constants. The differential equation describing $Y_2(y)$ is

$$\frac{Y_2''(y)}{Y_2(y)} + k^2 - \eta^2 = 0, \tag{4.158}$$

or

$$\frac{Y_2''(y)}{Y_2(y)} + \eta_y^2 = 0, \tag{4.159}$$

where

$$\eta_y^2 = k^2 - \eta^2. \tag{4.160}$$

The solution to equation (4.159) is given by

$$Y_2(y) = c_9 \cos(\eta_y y) + c_{10} \sin(\eta_y y), \tag{4.161}$$

here, c_9 and c_{10} represent arbitrary constants.

From equation (4.152) and equation (4.161),

$$Y_2(y) = \cos\left(\frac{n\pi}{b}\right), \tag{4.162}$$

where $\eta_y = \dfrac{n\pi}{b}$ is the eigenvalue obtained from equation (4.162) by applying the boundary conditions. Whereas, for $X_2(x)$ the ordinary differential equation is

$$\frac{X_2''(x)}{X_2(x)} + \eta_x^2 = 0, \tag{4.163}$$

where

$$\eta^2 = k^2 - \eta^2 - \eta_y^2. \tag{4.164}$$

The solution of equation (4.163) is given by

$$X_2(x) = c_{11}\cos(\eta_x x) + c_{12}\sin(\eta_x x), \tag{4.165}$$

where c_{11} and c_{12} denote arbitrary constants. Combining equation (4.165) and equation (4.152),

$$X_2(x) = \cos\left(\frac{m\pi}{a}\right), \tag{4.166}$$

where $\eta_x = \dfrac{m\pi}{a}$ is the eigenvalue obtained from equation (4.166) by applying the boundary conditions. For supperposition principal, the total field potential in region II, we can write as

$$\phi_2^a(x,y,z) = \sum_{m=0}^{\infty}\sum_{n=0}^{\infty}(C_{mn}^a e^{i\eta_{mn}z} + D_{mn}^a e^{-i\eta_{mn}z})\psi_{mn}(x,y), \tag{4.167}$$

where $\psi_{mn}(x,y)$ represents the eigenfunction in region II, given by

$$\psi_{mn}(x,y) = \cos\left(\frac{m\pi}{a}x\right)\cos\left(\frac{n\pi}{b}y\right). \tag{4.168}$$

Here, η_{mn} represents the wave number of the $(mn)^{th}$ mode, as determined by equation (4.164), and is given by

$$\eta_{mn} = \sqrt{k^2 - \left(\frac{m\pi}{a}\right)^2 - \left(\frac{n\pi}{b}\right)^2}. \tag{4.169}$$

It is important to note that $A^a_{mn}, B^a_{mn}, C^a_{mn}$, and D^a_{mn} are unknown coefficients. Assuming a fundamental duct mode with unit amplitude propagating from region II in the positive z-direction, we consider only transmission in region II by setting $D^a_{mn} = 0$ in equation (4.86). The fluid potential

$$\phi^a_1(x,y,z) = \sum_{m=0}^{\infty}\sum_{n=0}^{\infty}(A^a_{mn}e^{i\eta_{mn}(z+\ell)} + B^a_{mn}e^{-i\eta_{mn}(z+\ell)})\psi_{mn}(x,y), \tag{4.170}$$

and

$$\phi^a_2(x,y,z) = \sum_{m=0}^{\infty}\sum_{n=0}^{\infty}(C^a_{mn}e^{i\eta_{mn}z} + D^a_{mn}e^{-i\eta_{mn}z})\psi_{mn}(x,y). \tag{4.171}$$

At $z = 0$, the presence of a rigid wall leads to

$$\phi^a(x,y) = 0, \quad z = 0. \tag{4.172}$$

Substuting equation (4.171) into equation (4.172), we may get

$$\phi^a_2(x,y,z) = \sum_{m=0}^{\infty}\sum_{n=0}^{\infty}(C^a_{mn} + D^a mn)\psi_{mn}(x,y), \tag{4.173}$$

The result of simplification is

$$-C^a_{mn} = D^a_{mn}. \tag{4.174}$$

Substuting the value of D^a_{mn}, from equation (4.174) into equation (4.173), we get

$$\phi^a_2(x,y,z) = \sum_{m=0}^{\infty}\sum_{n=0}^{\infty}(i2C^a_{mn}\sin(\eta_{mn}\ell)\psi_{mn}(x,y). \tag{4.175}$$

Once the excitation coefficient A^a_{mn} is specified for duct mode excitation, the coefficients C^a_{mn} and B^a_{mn} become the unknown quantities.

The dynamics of the membrane located at $z = -\ell$ are then examined using the Galerkin method, which allows us to solve for the unknown amplitudes

4.7 Galerkin Formulation for Elastic Plate ynamics

The dynamical response of plate at interface $z = -\ell$ in harmonic time dependence

$$\Delta^4 w^a - \mu^4 w^a = \alpha(\phi_1^a - \phi_2^a), \tag{4.176}$$

where

$$\mu = \frac{\rho_{eff}\omega^2 h}{D_p}, \tag{4.177}$$

and

$$\alpha = \frac{i\omega\rho}{D_p}. \tag{4.178}$$

and α are structure wave number

$w(x, y)e^{i\omega t} = 0$, Subject to the boundary condition that

$$w^a(0, y) = 0, \tag{4.179}$$

$$w^a(a, y) = 0, \tag{4.180}$$

$$\frac{\partial^2 w^a}{dx^2}(0, y) = 0, \tag{4.181}$$

$$\frac{\partial^2 w^a}{dx^2}(a, y) = 0, \tag{4.182}$$

$$w^a(x, 0) = 0, \tag{4.183}$$

$$w^a(x, b) = 0, \tag{4.184}$$

$$\frac{\partial^2 w^a}{dy^2}(x, 0) = 0, \tag{4.185}$$

$$\frac{\partial^2 w^a}{dy^2}(x, b) = 0. \tag{4.186}$$

Now we can construct the eigenvalue problem associated with equation (4.176) to equation (4.186), given as follows

$$(\Delta^4 - \lambda_{mn}^4)\phi_{mn}^a = 0, \tag{4.187}$$

$$\phi^a_{mn}(0,y) = 0, \tag{4.188}$$

$$\phi^a_{mn}(a,y) = 0, \tag{4.189}$$

$$\phi^{a\prime\prime}{}_{mn}(0,y) = 0, \tag{4.190}$$

$$\phi^{a\prime\prime}{}_{mn}(a,y) = 0, \tag{4.191}$$

$$\phi^a_{mn}(x,0) = 0, \tag{4.192}$$

$$\phi^a_{mn}(x,b) = 0, \tag{4.193}$$

$$\phi^{a\prime\prime}{}_{mn}(x,0) = 0, \tag{4.194}$$

$$\phi^{a\prime\prime}{}_{mn}(x,b) = 0. \tag{4.195}$$

The solution of equation (4.187) to equation (4.195) is as given below

$$\phi^a_{mn}(x,y) = \sin\left(\frac{m\pi}{a}x\right)\sin\left(\frac{n\pi}{b}y\right), \tag{4.196}$$

where

$$\lambda^2_{mn} = \left(\frac{m\pi}{a}\right)^2 + \left(\frac{n\pi}{b}\right)^2. \tag{4.197}$$

The function ϕ^a_{1mn} are orthogonal and satisfies orthogonality relation,

$$\int_0^a \int_0^b \phi^a_{1mn}\phi^a_{1pq}dxdy = E_p\delta_{mp}F_q\delta_{nq}. \tag{4.198}$$

Now we project the solution orthogonal basis as

$$w^a(x,y) = \sum_{m=0}^{\infty}\sum_{n=0}^{\infty} g^a_{mn}\phi^a_{mn}. \tag{4.199}$$

Using the value of equation (4.199), equation (4.170) and equation (4.175) into equation (4.93)

$$\sum_{m=0}^{\infty}\sum_{n=0}^{\infty}(\lambda^4_{mn} - \mu^4)g^a_{mn}\phi^a_{mn} = \alpha\sum_{m=0}^{\infty}\sum_{n=0}^{\infty}(A^a_{mn} + B^a_{mn} - 2C^a_{mn}\sin(\eta_{mn}z))\psi_{mn}(x,y), \tag{4.200}$$

Multiplying with ϕ_{1pq} and integrating from $0 < x < a$ and $0 < y < b$ we may get

$$g^a_{pq} = \frac{\alpha}{(\lambda^4_{pq} - \mu^4)E_pF_q} \sum_{m=0}^{\infty}\sum_{n=0}^{\infty}(A^a_{pq}e^{i\eta_{pq}(z+\ell)} + B^a_{pq}e^{-i\eta_{pq}(z+\ell)} + i2C^a_{mn}\sin(\eta_{pq}z))\Delta_{pq}, \tag{4.201}$$

where

$$\Delta_{pq} = \int_0^a \int_0^b \phi^a_{1pq}\psi_{pq}(x,y). \tag{4.202}$$

In region I, at $z = -\ell$, the following condition holds

$$\frac{\partial\phi^a_1}{\partial z} = w^a(x,y). \tag{4.203}$$

Using equation (4.170) and equation (4.199) into equation (4.203) we get

$$i\sum_{m=0}^{\infty}\sum_{n=0}^{\infty}(A^a_{mn} - B^a_{mn})\eta_{mn}\psi_{mn}(x,y) = \sum_{m=0}^{\infty}\sum_{n=0}^{\infty} g^a_{mn}\phi^a_{mn}. \tag{4.204}$$

Multiplying with ψ^a_{1pq} and integrating from $0 < x < a$ and $0 < y < b$ we obtain

$$A^a_{pq} - B^a_{pq} = \frac{1}{i\eta_{pq}E_pF_q}\sum_{m=0}^{\infty}\sum_{n=0}^{\infty} g^a_{pq}\int_0^a\int_0^b \phi^a_{1pq}\psi^a_{1pq}dxdy, \tag{4.205}$$

or

$$A^a_{pq} - B^a_{pq} = \frac{1}{i\eta_{pq}E_pF_q}\sum_{m=0}^{\infty}\sum_{n=0}^{\infty} g^a_{pq}\Delta_{pq}, \tag{4.206}$$

where

$$\Delta_{pq} = \int_0^a\int_0^b \phi^a_{1pq}\psi^a_{1pq}(x,y). \tag{4.207}$$

Likewise, in region II at $z = -\ell$, we have

$$\frac{\partial\phi^a_2}{\partial z} = w^a(x,y). \tag{4.208}$$

Using equation (4.175) and equation (4.199) into equation (4.208) we get

$$\sum_{m=0}^{\infty}\sum_{n=0}^{\infty} i2C^a_{mn}\eta_{mn}\cos(\eta_{mn\ell})\psi_{mn}(x,y) = \sum_{m=0}^{\infty}\sum_{n=0}^{\infty} g^a_{mn}\phi^a_{mn}. \tag{4.209}$$

Multiplying with ψ^a_{2pq} and integrating from $0 < x < a$ and $0 < y < b$ we obtain

$$C_{pq}^{a} = \frac{1}{i2\cos\eta_{pq}E_pF_q}\sum_{m=0}^{\infty}\sum_{n=0}^{\infty} g_{pq}^{a}\int_0^a\int_0^b \phi_{2pq}^{a}\psi_{2pq}^{a}dxdy, \tag{4.210}$$

or

$$C_{pq}^{a} = \frac{1}{i2\cos\eta_{pq}E_pF_q}\sum_{m=0}^{\infty}\sum_{n=0}^{\infty} g_{pq}^{a}\epsilon_{pq}, \tag{4.211}$$

where

$$\epsilon_{pq} = \int_0^a\int_0^b \phi_{1pq}^{a}\psi_{pq}^{a}(x,y). \tag{4.212}$$

4.7.1 Numerical Solution

In the soft wall-backed configuration, the formulation from Section 4.7 is solved in *Mathematica* with $N = 16$ modal terms, using the same geometric and fluid parameters as in the rigid wall case: $a = 4000$, $b = 6000$, $L = 2000$, $\rho_0 = 1.23$, $c_0 = 343$. Due to the soft termination, the computed normal velocity amplitudes at $z = -\ell$ are significantly larger than in the rigid wall case, particularly for the lower modes. The pressure field distribution indicates a greater amount of acoustic energy transmitted into the plate, which results in broader and deeper absorption dips in the frequency response.

The soft wall condition effectively lowers the resonance frequencies and increases the bandwidth of strong coupling between the acoustic field and the plate vibrations, thereby improving the noise reduction capability over a wider frequency range. The results demonstrate that the soft boundary promotes stronger acoustic-structure interaction compared to the rigid case. The smoother variation of velocity and pressure with frequency produces a more stable absorption profile, which reduces sharp resonance effects. This means that the soft wall-backed configuration is better suited for practical noise control applications, as it provides effective attenuation not only at specific resonance frequencies but also across a wider portion of the spectrum. Figure (4.9) shows that the real parts of the dimensionless normal velocities $\phi_{1z}^{a}(x,y,z)$ and $\phi_{2z}^{a}(x,y,z)$ plotted over x and y at $z = -L$ for the soft-backed cavity. Both functions behave similarly, which agrees with the continuity condition of normal velocities at that surface.

Figure (4.10)presents the imaginary parts of $\phi^a 1z(x, y, z)$ and $\phi^a 2z(x, y, z)$ at the same location. These also show matching behavior, again consistent with the expected continuity condition. Furthermore, the agreement in the imaginary components confirms that the phase information is properly maintained across the interface. This observation provides additional verification of the accuracy of the mode-matching formulation.

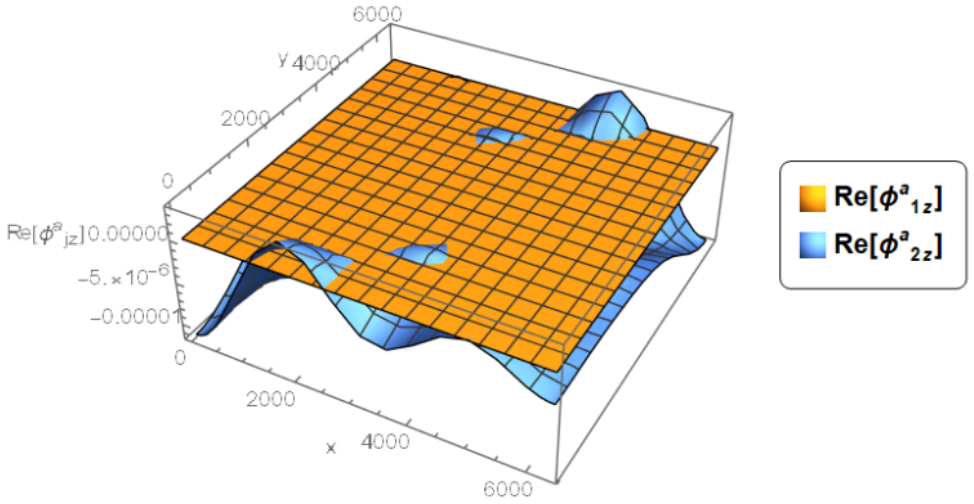

FIGURE 4.9: The real component of dimensionless normal velocities $\phi_1^a(x, y, z)$ and $\phi_2^a(x, y, z)$ against x and y at z=$-\ell$, where $\bar{a} = 4000, \bar{b} = 6000, \bar{L} = 2000$ and N =16 term (anti-Symmetric case)

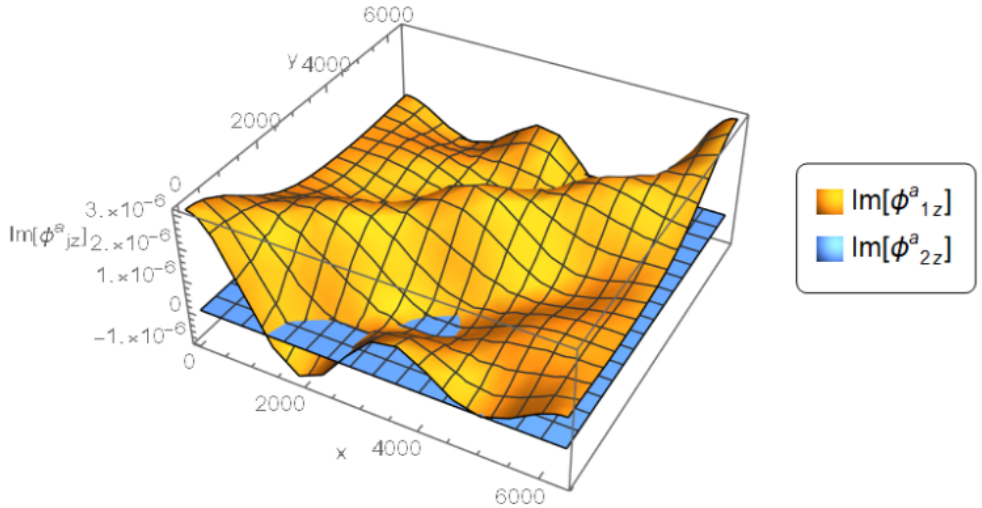

FIGURE 4.10: The imaginary component of dimensionless normal velocities $\phi_1^a(x, y, z)$ and $\phi 2^a(x, y, z)$ against x and y at z=$-\ell$, where $\bar{a} = 4000, \bar{b} = 6000, \bar{L} = 2000$ and N =16 term (anti-Symmetric case)

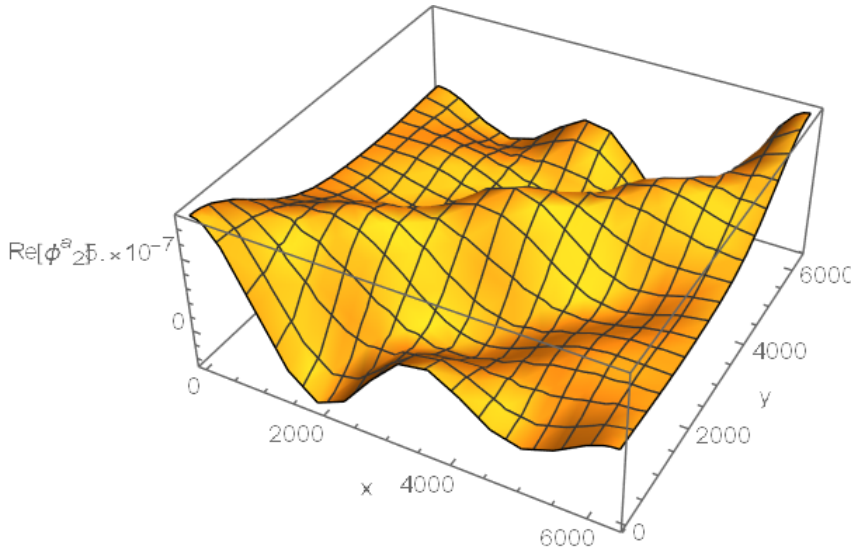

FIGURE 4.11: The real component of dimensionless pressure $\phi_2^a(x, y, z)$ against x and y at z=$-\ell$, where $\bar{a} = 4000, \bar{b} = 6000, \bar{L} = 2000$ and N =16 term (anti-Symmetric case)

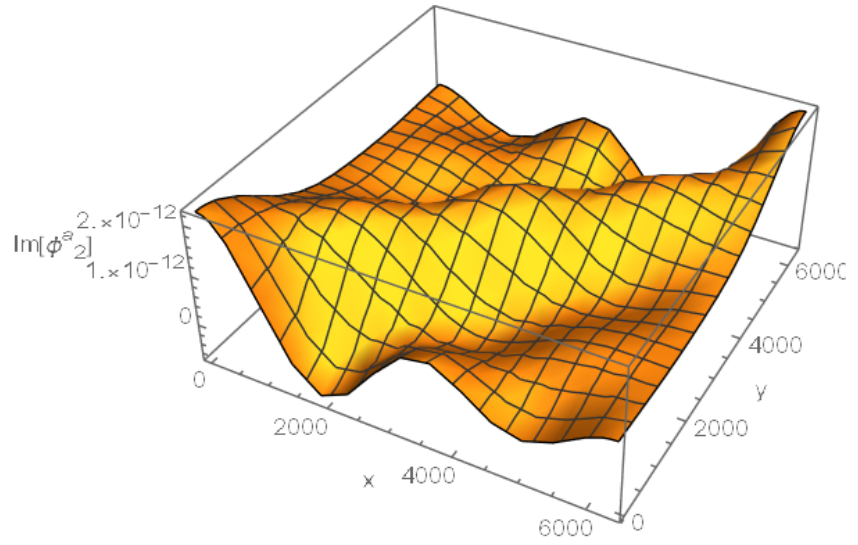

FIGURE 4.12: The imaginary component of dimensionless pressure $\phi_2^a(x, y, z)$ against x and y at z=$-\ell$, where $\bar{a} = 4000, \bar{b} = 6000, \bar{L} = 2000$ and N =16 term (anti-Symmetric case)

Figure (4.11) shows the real part of the dimensionless acoustic pressure at . The surface pattern reveals an oscillating behavior, demonstrating the presence of multiple interacting wave modes within the duct. These pressure fluctuations correspond to the anti-symmetric excitation conditions and soft wall boundaries. The alternating high and low values indicate regions of constructive and destructive interference, contributing to a complex acoustic field inside the cavity. Figure

(4.12) shows the imaginary part of the pressure field at the same interface. The smooth undulations in the graph highlight phase differences caused by the wave propagation. This component reflects the system's capacity to store reactive energy during vibration. The varying phase across the surface is typical of soft wall conditions, and the anti-symmetric case further emphasizes the asymmetry in the distribution, affecting the total acoustic response.

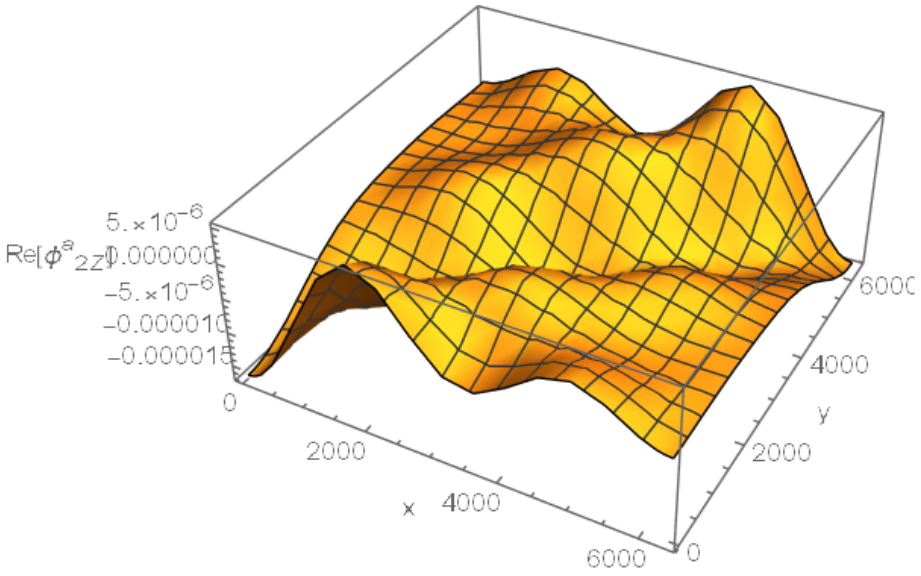

FIGURE 4.13: The real component of dimensionless normal velocity $\phi_2^a(x, y, z)$ against x and y at z=0, where $\bar{a} = 4000, \bar{b} = 6000, \bar{L} = 2000$ and N =16 term (anti-Symmetric case)

Figure (4.13) displays the real component of the normal velocity at , the surface of the elastic plate. The fact that the velocity is clearly non-zero confirms the nature of the soft wall, which permits vertical movement of the structure. In contrast to rigid boundaries, which prevent normal motion, the soft interface supports vibration. The anti-symmetric excitation results in an uneven velocity profile, influencing how the plate dynamically interacts with the acoustic field and transmits energy into the surrounding medium. Figure (4.14) presents the imaginary part of the dimensionless normal velocity at , which is the interface where the elastic plate is located. The plot indicates clear variations in phase across the plate surface, confirming that the structure is undergoing dynamic motion. The presence of non-zero imaginary values reflects the system's reactive behavior, meaning part of the energy is temporarily stored in the vibrating plate.

This outcome is consistent with the soft wall condition, which permits the plate

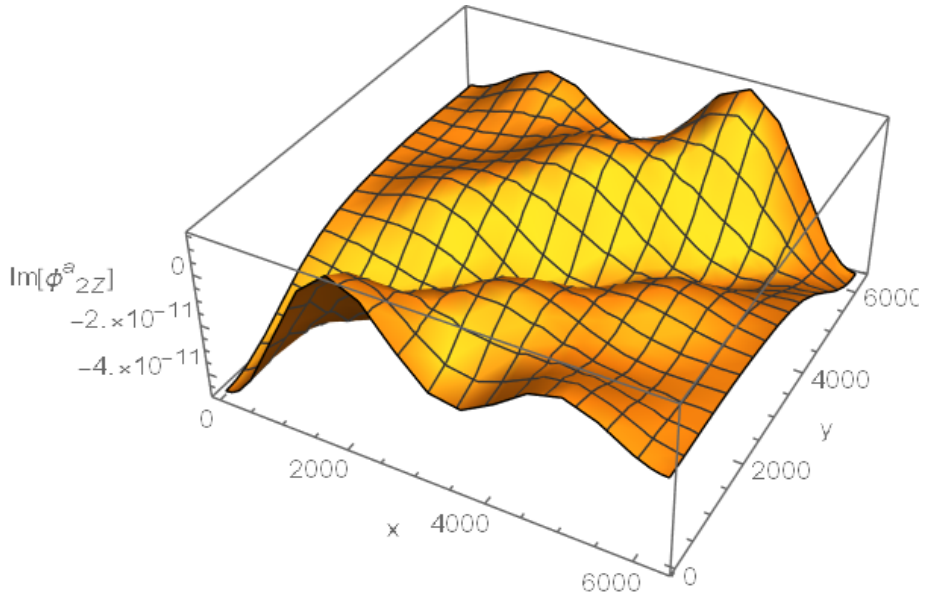

FIGURE 4.14: The imaginary component of dimensionless normal velocity $\phi_2^a(x, y, z)$ against x and y at z=0, where $\bar{a} = 4000, \bar{b} = 6000, \bar{L} = 2000$ and N =16 term (anti-Symmetric case)

to move in response to the acoustic excitation. The anti-symmetric excitation leads to an uneven distribution of velocity phases, influencing both the structural response and the acoustic field within the cavity.

Chapter 5

Conclusion

In this work, the acoustic impedance of an elastic panel placed inside a rigid rectangular waveguide was evaluated. The pressure difference across the panel was expressed as a sine series, and the panel response was described using modal amplitudes.

To determine these modal amplitudes, the governing equation was multiplied by appropriate sine functions and integrated over the surface, following the Galerkin method.

This led to a system of equations that allowed the average velocity of the panel to be calculated. Finally, the acoustic impedance was obtained by taking the ratio of the pressure difference to the average velocity.

Furthermore, the scattering behavior of an elastic plate placed inside a 3D rectangular waveguide was analyzed. The fluid potential in the waveguide was modeled using modal expansions with sine functions, and the plate's response was described using a double sine series.

The governing equation of the plate was coupled with the surrounding acoustic fields through the Galerkin method, which helped convert the problem into a solvable system of equations. Appropriate boundary conditions were applied to ensure soft-wall behavior, allowing vertical motion of the plate. Numerical simulations shows how the acoustic pressure and normal velocity distributions vary across the waveguide, confirming the wave-structure interaction. The results showed clear

patterns of phase shift and vibration, consistent with anti-symmetric excitation and energy storage within the structure.

Bibliography

[1] L. E. Kinsler, A. R. Frey, A. B. Coppens, and V. Sanders. *Fundamentals of Acoustics*. Wiley, 4th edition, 2000.

[2] D. Y. Maa. Potential of microperforated panel absorber. *Journal of the Acoustical Society of America*, 104(5):2861–2866, 1998.

[3] L. Beranek and T. Mellow. *Acoustics: Sound Fields and Transducers*. Academic Press, 2012.

[4] A. W. Leissa. *Vibration of Plates*. NASA SP-160, 1969.

[5] S. S. Rao. *Vibration of Continuous Systems*. John Wiley & Sons, 2007.

[6] S. W. Ren, L. V. Belle, C. Claeys, F. X. Xin, T. J. Lu, E. Deckers, and W. Desmet. Improvement of the sound absorption of flexible micro-perforated panels by local resonances. *Mechanical Systems and Signal Processing*, 117: 138–156, 2019.

[7] W. Y. Yeang, D. Halim, X. Yi, and H. Chen. On improving low-frequency sound absorption using a compound microperforated panel backed by a panel-type resonator with tuned multi-frequency resonators. *Journal of Sound and Vibration*, 570:118134, 2024.

[8] W. Y. Yeang, D. Halim, X. Yi, and H. Chen. A compound microperforated panel backed by a panel-type resonator with a helmholtz neck and multi-frequency resonators to improve bandwidth and low frequency sound absorption. *Applied Acoustics*, 221:110030, 2024.

[9] Y. Zhang, G. Wang, Z. Zhu, and Q. Liu. Vibro-acoustic coupling characteristics of the microperforated panel with local resonators. *International Journal of Mechanical Sciences*, 245:108125, 2023.

[10] R. L. Mu, M. Toyoda, and D. Takahashi. Sound insulation characteristics of multi-layer structures with a microperforated panel. *Applied Acoustics*, 72 (11):849–855, 2011.

[11] X.L. Gai, T. Xing, X.H. Li, B Zhang, and W. J. Wang. Sound absorption of microperforated panel mounted with helmholtz resonators. *Applied Acoustics*, 114:260–265, 2016.

[12] K. Sakagami, M. Morimoto, and W. Koike. A numerical study of double-leaf microperforated panel absorbers. *Applied acoustics*, 67(7):609–619, 2006.

[13] A. I. Mosa and R .and Esraa A.A. Putra, A .and Ramlan. Wideband sound absorption of a double-layer microperforated panel with inhomogeneous perforation. *Applied Acoustics*, 161:107167, 2020.

[14] I. Prasetiyo, I. Sihar, and A. S. Sudarsono. Realization of a thin and broadband microperforated panel (mpp) sound absorber. *Applied Acoustics*, 183: 108295, 2021.

[15] M. Toyoda and D. Eto. Prediction of microperforated panel absorbers using the finite-difference time-domain method. *Wave Motion*, 86:110–124, 2019.

[16] P.S. Ma, H.S. Kim, S.H. Lee, and Y.H. Seo. Quasi-perfect absorption of broadband low-frequency sound in a two-port system based on a micro-perforated panel resonator. *Applied Acoustics*, 186:108449, 2022.

[17] X. Liu, C. Wang, Y. Zhang, and L. Huang. Investigation of broadband sound absorption of smart micro-perforated panel (mpp) absorber. *International Journal of Mechanical Sciences*, 199:106426, 2021.

[18] Y. Zhang, Z. Zhu, Z. Sheng, Y. He, and G. Wang. Sound absorption properties of the metamaterial curved microperforated panel. *International Journal of Mechanical Sciences*, 268:109003, 2024.

[19] Z. Hashemi, N. Asadi, M. Sadeghian, A. Putra, S. Ahmadi, M. Alidosti, and M. J. SheikhMozafari. Optimization and comparative analysis of micro-perforated panel sound absorbers: A study on structures and performance enhancement. *Measurement*, 236:115123, 2024.

[20] Y. Qian, K. Cui, S. Liu, Z. Li, D. Kong, and S. Sun. Numerical study of the acoustic properties of micro-perforated panels with tapered hole. *Noise Control Engineering Journal*, 62(3):152–159, 2014.

[21] X.L. Gai, T. Xing, X.H. Li, B. Zhang, F. Wang, Z.N. Cai, and Y. Han. Sound absorption of microperforated panel with l shape division cavity structure. *Applied Acoustics*, 122:41–50, 2017.

[22] M. Toyoda, R. L. Mu, and D. Takahashi. Relationship between helmholtz-resonance absorption and panel-type absorption in finite flexible microperforated-panel absorbers. *Applied Acoustics*, 71(4):315–320, 2010.

[23] K. Sakagami, I. Yamashita, M. Yairi, and M. Morimoto. Effect of a honeycomb on the absorption characteristics of double-leaf microperforated panel (mpp) space sound absorbers. *Noise Control Engineering Journal*, 59(4):363–371, 2011.

[24] Z. Xu, W. He, X. Peng, F. Xin, and T. J. Lu. Sound absorption theory for micro-perforated panel with petal-shaped perforations. *The Journal of the Acoustical Society of America*, 148(1):18–24, 2020.

[25] W. Guo and H. Min. A compound micro-perforated panel sound absorber with partitioned cavities of different depths. *Energy Procedia*, 78:1617–1622, 2015.

[26] F. Arndt. Mode-matching methods. *Encyclopedia of RF and Microwave Engineering*, 2005.

[27] A. Kirilenko, D. Kulik, Y. Parkhomenko, L. Rud, and V. Tkachenko. Automatic electromagnetic solvers based on mode-matching, transverse resonance, and s-matrix techniques. In *14th International Conference on Microwaves,*

Radar and Wireless Communications. MIKON-2002. Conference Proceedings (IEEE Cat. No. 02EX562), volume 3, pages 815–824. IEEE, 2002.

[28] A. Dreher. Discrete mode matching for the full-wave analysis of planar waveguide structures. In *1996 IEEE MTT-S International Microwave Symposium Digest*, volume 1, pages 193–196. IEEE, 1996.

[29] L. Polo-López, J. A. Ruiz, C., J.é R. Montejo-Garai, and Jesús M Rebollar. Analysis of waveguide devices involving lateral and transverse perfect magnetic wall boundary conditions by the mode-matching method. *Radio Science*, 52(9):1223–1234, 2017.

[30] C. Vale and P. Meyer. Automated intelligent mode selection for fast mode matching analysis of waveguide discontinuities. In *2001 IEEE MTT-S International Microwave Sympsoium Digest (Cat. No. 01CH37157)*, volume 3, pages 1949–1952. IEEE, 2001.

[31] O. P. Franza and W. C. Chew. Recursive mode matching method for multiple waveguide junction modeling. *IEEE transactions on microwave theory and techniques*, 44(1):87–92, 1996.

[32] S. Llorente, R., B. Gimeno, and M. Salazar, P. Analysis of cylindrical geometries in rectangular waveguides using mode matching. In *2005 European Microwave Conference*, volume 2, pages 4–pp. IEEE, 2005.

[33] Wikipedia contributors. Acoustics, 2025. URL https://en.m.wikipedia.org/wiki/Acoustics. Definition and acoustic wave equation.

[34] Frank M. White. *Fluid Mechanics*. McGraw-Hill Education, 7th edition, 2011. Conservation of mass and momentum equations in fluid dynamics.

[35] Wikipedia contributors. Conservation of mass and momentum, 2025. URL https://en.wikipedia.org/wiki/Conservation_of_mass. Definitions and governing equations.

[36] H. P. Lee and J. Pan. Recent developments in micro-perforated panel absorbers: A review. *Applied Acoustics*, 117:73–89, 2017. doi: 10.1016/j.apacoust.2016.10.005.

[37] Trevor J. Cox and Peter D'Antonio. *Acoustic Absorbers and Diffusers: Theory, Design and Application*. CRC Press, 2nd edition, 2009. ISBN 978-0-415-43728-4.

[38] Philip M. Morse and K. Uno Ingard. *Theoretical Acoustics*. Princeton University Press, 1968. ISBN 978-0691080003.

[39] David Halliday, Robert Resnick, and Jearl Walker. *Fundamentals of Physics*. John Wiley & Sons, 10th edition, 2013. ISBN 978-1118230718.

[40] Daniel J. Inman. *Engineering Vibration*. Pearson, 4th edition, 2014. ISBN 978-0132871693.

[41] J. Lee, S. Kim, and H. Park. Acoustic performance of metamaterial-based micro-perforated panels. *Journal of Sound and Vibration*, 480:115363, 2020.